De novo variants in the *PSMC3* proteasome AAA-ATPase subunit gene cause neurodevelopmental disorders associated with type I interferonopathies

Frédéric Ebstein[1,53], Sébastien Küry[2,3,53], Victoria Most[4], Cory Rosenfelt[5], Marie-Pier Scott-Boyer[6], Geeske M. van Woerden[7,8,9], Thomas Besnard[2,3], Jonas Johannes Papendorf[1], Maja Studencka-Turski[1], Tianyun Wang[10,47], Tzung-Chien Hsieh[11], Richard Golnik[12], Dustin Baldridge[13], Cara Forster[14], Charlotte de Konink[7,8], Selina M.W. Teurlings[7,8], Virginie Vignard[2,3], Richard H. van Jaarsveld[15], Lesley Ades[16,17], Benjamin Cogné[2,3], Cyril Mignot[18,19], Wallid Deb[2,3], Marjolijn C.J. Jongmans[15,20], F. Sessions Cole[13], Marie-José H. van den Boogaard[15], Jennifer A. Wambach[13], Daniel J. Wegner[13], Sandra Yang[14], Vickie Hannig[21], Jennifer Ann Brault[21], Neda Zadeh[22], Bruce Bennetts[23,24], Boris Keren[25], Anne-Claire Gélineau[25], Zöe Powis[26], Meghan Towne[26], Kristine Bachman[27], Andrea Seeley[27], Anita E. Beck[28], Jennifer Morrison[29], Rachel Westman[30], Kelly Averill[31], Theresa Brunet[32,33], Judith Haasters[34], Melissa T. Carter[35], Matthew Osmond[36], Patricia G. Wheeler[37], Francesca Forzano[38], Shehla Mohammed[38], Yannis Trakadis[39], Andrea Accogli[39], Rachel Harrison[40], Deciphering Developmental Disorders Study[41], Care4Rare Canada Consortium[42], Sophie Rondeau[43], Geneviève Baujat[43], Giulia Barcia[43], René Günther Feichtinger[44], Johannes Adalbert Mayr[44], Martin Preisel[44], Frédéric Laumonnier[45,46], Alexej Knaus[11], Bertrand Isidor[2,3], Peter Krawitz[10], Uwe Völker[47], Elke Hammer[47], Arnaud Droit[6], Evan E. Eichler[10,48], Ype Elgersma[8,9], Peter W. Hildebrand[4,49,50], François Bolduc[5,51,52,53], Elke Krüger[1,54,#] and Stéphane Bézieau[2,3,54,#]

[1]Institut für Medizinische Biochemie und Molekularbiologie (IMBM), Universitätsmedizin Greifswald, Ferdinand-Sauerbruch-Straße, 17475 Greifswald, Germany;

[2]CHU Nantes, Service de Génétique Médicale, 44093 Nantes, France;

[3]l'Institut du Thorax, INSERM, CNRS, Université de Nantes, Nantes, France;

[4]Institut für Medizinische Physik und Biophysik, Universität Leipzig, Medizinische Fakultät, Härtelstr. 16-18, 04107 Leipzig, Germany;

[5]Department of Pediatrics, University of Alberta, Edmonton, AB, Canada;

[6]Research Center of Quebec CHU-Université Laval, Québec, QC PQ G1E6W2, Canada;

[7]Department of Neuroscience, Erasmus University Medical Center, 3015 CN, Rotterdam, The Netherlands;

[8]ENCORE Expertise Center for Neurodevelopmental Disorders, Erasmus University Medical Center, 3015 CN, Rotterdam, The Netherlands;

[9]Department of Clinical Genetics, Erasmus University Medical Center, 3015 CN, Rotterdam, The Netherlands

[10]Department of Genome Sciences, University of Washington School of Medicine, Seattle, WA 98195, USA;

[11]Institute for Genomic Statistics and Bioinformatics, University Hospital Bonn, Rheinische Friedrich-Wilhelms-Universität Bonn, Bonn, Germany;

[12]Klinik für Pädiatrie I, Universitätsklinikum Halle (Saale), 06120 Halle (Saale);

[13]The Edward Mallinckrodt Department of Pediatrics, Washington University School of Medicine, St. Louis, MO, USA;

[14]GeneDx, 207 Perry Parkway, Gaithersburg, MD 20877, USA;

[15]Department of Genetics, University Medical Center Utrecht, Utrecht, The Netherlands;

[16]Department of Clinical Genetics, The Children's Hospital at Westmead, Locked Bag 4001, Westmead, NSW, 2145, Australia;

[17]Disciplines of Genomic Medicine & Child and Adolescent Health, Faculty of Medicine and Health, University of Sydney, Sydney, NSW, 2145, Australia;

[18]APHP, Hôpital Pitié-Salpêtrière, Département de Génétique, Centre de Reference Déficience Intellectuelle de Causes Rares, GRC UPMC «Déficience Intellectuelle et Autisme», Paris, France;

[19]Sorbonne Universités, Institut du Cerveau et de la Moelle épinière, ICM, Inserm U1127, CNRS UMR 7225, F-75013, Paris, France;

[20]Princess Máxima Center for Pediatric Oncology, Utrecht, The Netherlands;

[21]Department of Medicine, Vanderbilt University Medical Center, Nashville, Tennessee, USA;

[22]Genetics Center, Orange, CA 92868, USA; Division of Medical Genetics, Children's Hospital of Orange County, Orange, CA 92868, USA;

[23]Disciplines of Genomic Medicine & Child and Adolescent Health, Faculty of Medicine and Health, University of Sydney, Sydney, NSW, 2145, Australia;

[24]Sydney Genome Diagnostics, Western Sydney Genetics Program, The Children's Hospital at Westmead, Sydney, NSW, Australia;

[25]Département de Génétique, Centre de Référence des Déficiences Intellectuelles de Causes Rares, Groupe Hospitalier Pitié-Salpêtrière, Assistance Publique-Hôpitaux de Paris, 75013 Paris;

[26]Department of Clinical Research, Ambry Genetics, Aliso Viejo, CA 92656, USA;

[27]Genomic Medicine Institute, Geisinger, Danville, PA, USA;

[28]Department of Pediatrics, Division of Genetic Medicine, University of Washington & Seattle Children's Hospital, Seattle, WA, USA;

[29]Division of Genetics, Arnold Palmer Hospital for Children, Orlando Health, Orlando, FL 32806, USA;

[30]Division of Genetics, St. Luke's Clinic, Boise, ID, USA;

[31]UT Health Science Center at San Antonio, Department of Pediatrics, Division of Pediatric Neurology, San Antonio, TX 78229, USA;

[32]Institute of Human Genetics, Technical University of Munich, School of Medicine, 81675 Munich, Germany;

[33]Institute of Neurogenomics (ING), Helmholtz Zentrum München, German Research Center for Environmental Health, 85764 Neuherberg, Germany;

[34]Klinikum der Universität München, Integriertes Sozial- pädiatrisches Zentrum, 80337 Munich, Germany;

[35]Department of Genetics, Children's Hospital of Eastern Ontario, Ottawa, Ontario, Canada;

[36]Children's Hospital of Eastern Ontario Research Institute, University of Ottawa, Ottawa, Canada;

[37]Division of Genetics, Arnold Palmer Hospital for Children, Orlando Health, Orlando, FL 32806, USA;

[38]Clinical Genetics Department, Guy's & St Thomas' NHS Foundation Trust, London, UK;

[39]Division of Medical Genetics, McGill University Health Centre, Montreal, QC, Canada;

[40]Department of Clinical Genetics, Nottingham University Hospitals NHS Trust, City Hospital Campus, The Gables, Gate 3, Hucknall Road, Nottingham, NG5 1PB, UK;

[41]Wellcome Trust Sanger Institute, Wellcome Trust Genome Campus, Hinxton, Cambridge, UK.

[42]Children's Hospital of Eastern Ontario Research Institute, University of Ottawa, Canada;

[43]Service de Médecine Génomique des Maladies Rares, Hôpital Universitaire Necker-Enfants Malades, 75743 Paris, France;

[44]University Children’s Hospital, Salzburger Landeskliniken (SALK) and Paracelsus Medical University (PMU), Salzburg, Austria;

[45]UMR 1253, iBrain, Université de Tours, Inserm, Tours, France;

[46]Service de Génétique, Centre Hospitalier Régional Universitaire, Tours, France;

[47]Universitätsmedizin Greifswald, Interfakultäres Institut für Genetik und Funktionelle Genomforschung, Abteilung für Funktionelle Genomforschung, 17487 Greifswald, Germany;

[48]Howard Hughes Medical Institute, Seattle, WA, 98195, USA;

[49]Institute of Medical Physics and Biophysics, Charité University Medicine Berlin, Berlin, Germany;

[50]Berlin Institute of Health, Berlin, Germany;

[51]Neuroscience and Mental Health Institute, University of Alberta, Edmonton, AB, Canada;

[52]Department of Medical Genetics, University of Alberta, Edmonton, AB, Canada;

[53]The authors equally contributed to this work.

[54]The authors equally contributed to this work.

[#]corresponding authors:

Professor Elke Krüger, Email: elke.krueger@uni-greifswald.de; Professor Stéphane Bézieau, Email: stephane.bezieau@chu-nantes.fr

Word count for the manuscript: 6292.

Abstract

A critical step in preserving protein homeostasis by the ubiquitin-proteasome system (UPS) is the recognition, binding, unfolding, and translocation of protein substrates by AAA-ATPase proteasome subunits for degradation by 26S proteasomes. Here, we identified fourteen different *de novo* missense variants in the *PSMC3* gene encoding the AAA-ATPase proteasome subunit Rpt5 in twenty-two unrelated heterozygous subjects with an autosomal dominant form of neurodevelopmental delay and intellectual disability. Indeed, depletion of *PSMC3* impaired reversal learning capabilities in a *Drosophila* model. The *PSMC3* variants cause proteasome dysfunction in patient-derived cells by disruption of substrate translocation, proteotoxic stress and proteostatic imbalances, as well as alterations in proteins controlling developmental and innate immune programs. Molecular analysis confirmed the induction of cellular stress responses and dysregulated mitophagy along with an elevated type I interferon (IFN) signature. Our data define *PSMC3* variants as the genetic cause of proteotoxic stress alerting the innate immune system to mount a type I IFN response and link neurodevelopmental syndromes to interferonopathies.

Word count for the Abstract: 160.

Introduction

Proteasomes are large multi-protein complexes whose structure is adapted to the function of protein degradation [1, 2]. Together with the autophagosomal-lysosomal system, it maintains protein homeostasis by counterbalancing the synthesis of new proteins by the translational machinery [3-6]. The proteasome is part of the ubiquitin-proteasome system (UPS) which counts numerous enzymes acting upstream of the proteasome [7, 8]. Aged or unstructured proteins are preliminary ubiquitin-tagged by the ubiquitination machinery through a cascade of enzymatic reactions [9, 10]. Ubiquitin modification is a signal recognized by the 26S proteasome which then takes in charge the hydrolysis of the substrate.

The 26S proteasome consists of two parts, the 20S core proteolytic particle and the 19S regulatory particle which caps the 20S particle at one and/or both ends [11, 12]. Briefly, polyubiquitinated proteins are recognized by the 19S regulatory particle where they are unfolded and deubiquitinated before their ATP-dependent translocation into the 20S core particle [13, 14]. There, proteins are hydrolyzed into small peptides by the β5, β1 and β2 catalytic subunits that exhibit chymotrypsin-, trypsin and caspase-like activities, respectively [15, 16]. Depending on the nature of the catalytic subunits, two major forms of proteasomes exist, namely the standard ones containing the β1, β2 and β5 catalytic standard subunits and the immunoproteasomes harboring the β1i, β2i and β5i inducible subunits [17]. While standard proteasomes are expressed in virtually all types of tissues, the expression of the inducible subunits is restricted to immune cells and non-immune cells exposed to type I and/or II interferons (IFN) [18, 19].

In more details, the 19S regulatory particle comprises two parts: a base and a lid. In the base, four regulatory particle non-ATPase subunits (*i.e.* Rpn1, Rpn2, Rpn10 and Rpn13) ensure recognition and capture of ubiquitin-modified substrates [20], whereas six AAA (ATPase Associated with various cellular Activities)-ATPase subunits, namely PSMC1-6 (also referred to as Rpt1-6) use the energy provided by ATP hydrolysis to unfold and

translocate the substrate into the 20S proteolytic core particle by gate opening [21]. The lid contains eight non-ATPase scaffolding subunits (Rpn3, Rpn5-9, Rpn12, and Rpn15) [22, 23], and the deubiquitinating enzyme (DUB) Rpn11 [24].

Pathogenic variants in proteasome subunit genes cause rare proteasomopathies with a broad spectrum of symptoms [25, 26]. So far, with the exception of the PSMB1 (i.e. β6) subunit [27], all pathogenic variants related to the 20S core particle have been shown to provoke immune dysregulation. Indeed, several genes encoding β-subunits (*PSMB4*, *PSMB8*, *PSMB9*, *PSMB10*), α-subunits (*PSMA3*) or assembly chaperone genes (*POMP, PSMG2)* of the 20S proteasome complex have been involved in autosomal recessive proteasome-associated autoinflammatory syndromes (PRAAS) [28-35]. By contrast, the only Mendelian disorder involving a gene of the 19S regulatory particle, the Stankiewicz-Isidor syndrome (MIM: 617516) caused by truncating variants of *PSMD12* (also referred to as Rpn5) is a neurodevelopmental polymalformative syndrome [36], recently associated with a mild interferonopathy (Isidor et al., in press).

In this work, we identify a series of fourteen dominant *de novo* variants in the *PSMC3* gene coding for the AAA-ATPase PSMC3/Rpt5. Rare missense variants were detected in twenty-two individuals presenting with neurodevelopmental delay (NDD) and/or intellectual disability (ID) together with various congenital malformations. Together, our data highlight interferonopathy as a potential contributor to the pathogenesis of NDD/ID in subjects carrying loss-of-function variants in subunits of the 19S proteasome regulatory particle.

185 ## Materials & Methods

186 ### Genetic studies and ethics statement

187 This study was approved by the CHU de Nantes ethics committee (Research Programme
188 "Génétique Médicale DC-2011-1399). Written informed consent was obtained from all study
189 participants, including probands and healthy parents. All affected individuals were initially
190 referred for unexplained developmental delay (DD) and/or intellectual disability (ID) together
191 with various congenital malformations. They underwent extensive clinical examination by at
192 least one expert clinical geneticist. Routine genetic testing was performed whenever clinically
193 relevant, including copy number variation (CNV) analysis by high-resolution array-based
194 comparative genomic hybridization (aCGH). As these tests provided no diagnosis, trio-based
195 whole exome sequencing (WES) was performed on a diagnostic or research setting
196 whenever parental samples were available.

197

198 ### Patient samples

199 Peripheral blood mononuclear cells (PBMC) used in this paper were isolated from blood
200 draws from patients and related healthy controls (father and/or mother of the proband).
201 Briefly, PBMC were isolated by PBMC spin medium gradient centrifugations (pluriSelect),
202 washed three times with PBS, frozen in FBS with 10% DMSO and stored in liquid nitrogen
203 for further use. In some experiments, collected PBMC were expanded in U-bottom 96-well
204 plates together with feeder cells using RPMI 1640 supplemented with 10% human AB serum
205 (both purchased from PAN-Biotech GmbH) in the presence of 150 U/ml IL-2 (Miltenyi Biotec)
206 and 1 µg/µl L-PHA (Sigma) following the procedure of Fonteneau et al. [37]. After 3-4 weeks
207 of culture, resting T cells were washed and frozen as dry pellets for further use.

208

209 ### SDS-PAGE and western-blot analysis

210 Cell pellets from resting T cell isolated from patients and related controls were lysed in equal
211 amounts of standard RIPA buffer (50 mM Tris pH 7.5, 150 mM NaCl, 2 mM EDTA, 1 mM N-
212 ethylmaleimide, 10 µM MG-132, 1% NP40, 0.1% SDS) and separated by 10 or 12.5% SDS-

PAGE before transfer to PVDF membranes (200V for 1h). After blocking (20-min exposure to 1X Roti®-Block at room temperature), membranes were probed with relevant primary antibodies overnight at 4°C under shaking. The anti-α6 (clone MCP20), anti-α7 (clone MCP72), anti-β1 (clone MCP421), anti-PSMC2 (BML-PW8315) and anti-PSMC3 (BML-PW8310) primary antibodies were purchased from Enzo Life Sciences. Primary antibodies specific for TCF11/Nrf1 (clone D5B10), ubiquitin (clone D9D5), GAPDH (clone 14C10), PINK1 (clone D8G3), BNIP3L/NIX (clone D8G3), LC3b (#2775), eIF2α (#9722), phospho-eIF2α (ser51, #119A11) were obtained from Cell Signaling Technology. The anti-PSMD12 antibody (clone H3) was a purchase from Santa Cruz Biotechnology Inc. The anti-PA28-α (K232/1) is laboratory stock and was used in previous studies [33]. Antibodies directed against β5 (ab3330), α-Tubulin (clone DM1A) and phospho-PKR (Thr446, clone E120) were purchased from Abcam. Following incubation with primary antibodies, membranes were washed three times with PBS/0.2% Tween and subsequently incubated with anti-mouse or –rabbit HRP conjugated secondary antibodies (1/5.000) for 1h at room temperature. Proteins were then visualized using an enhanced chemiluminescence detection kit (ECL) (Biorad).

Native PAGE and proteasome in-gel peptidase activity assay

Cell pellets from resting T cell isolated from patients and related controls were lysed in ice-cold homogenization TSDG buffer (10 mM Tris pH 7.0, 10 mM NaCl, 25 mM KCl, 1.1 mM $MgCl_2$, 0.1 mM EDTA, 2 mM DTT, 2 mM ATP, 1 mM NaN_3, 20 % Glycerol) and proteins were extracted using freeze/thawing in liquid nitrogen. Protein quantification of the soluble lysates was determined using a standard bicinchoninic acid assay (BCA) from Thermo Fisher Scientific. Twenty micrograms of whole-cell lysates were run on 3-12% gradient Bis-Tris gels (Thermo Fisher Scientific) at 45V overnight at 4°C using an electrophoresis buffer consisting of 50 mM BisTris and 50 mM Tricine (pH 6,8). Following separation, peptidase activity of the proteasome was measured by incubating the gels with 0.1 mM of the suc-LLVY-AMC fluorogenic peptide (Bachem) at 37°C for 20 min in an overlay buffer (20 mM Tris, 5 mM

240 $MgCl_2$, pH 7,0). Proteasome bands were subsequently visualized by exposing the gel to UV
241 light at 360 nm and detected at 460 nm using an Imager.
242
243 **RNA isolation, reverse-transcription and PCR analysis**
244 Total RNA was isolated from resting T cells using the kit from Analytic Jena AG following the
245 manufacturer's instructions. For subsequent real-time PCR, 100-500 ng of the isolated total
246 RNA was reverse transcribed using the M-MLV reverse transcriptase (Promega).
247 Quantitative PCR was performed using the Premix Ex Taq™ (probe qPCR purchased from
248 TaKaRa) and in duplicates to determine the mRNA levels of each IFN-stimulated gene (ISG)
249 using FAM-tagged TaqMan™ Gene Expression Assays obtained from Thermo Fisher
250 Scientific according to the manufacturer's instructions. TaqMan™ probes used in this study
251 for ISG quantification included *IFI27, IFI44L, IFIT1, ISG15, RSAD2, IFI44, MX1, OASL1,*
252 *CXCL9* and *CXCL10*. The cycle threshold (Ct) values for target genes were converted to
253 values of relative expression using the relative quantification (RQ) method ($2^{-\Delta\Delta Ct}$). Target
254 gene expression was calculated relative to Ct values for the GAPDH control housekeeping
255 gene.
256
257 **Behavioural studies**
258 Drosophila melanogaster (fruit flies) were raised on standard cornmeal-yeast media
259 developed at Cold Spring Harbor Laboratory in an incubator at 23°C with 40% humidity as
260 before [38]. Flies used for behaviour experiments included w1118 2202U (2U), Elav-Gal4.
261 and UAS-RNAi lines targeting PMSC3 orthologues. We identified the Drosophila ortholog of
262 PSMC3, Rpt5, using the DRSC Integrative Ortholog Prediction Tool
263 (https://www.flyrnai.org/diopt). UAS-Rpt5 RNAi (TRiP) lines were obtained from Bloomington
264 Drosophila Stock Center. We used the standard spatial restricted expression system Gal4-
265 UAS to pan-neuronally express (using pan-neuronal driver Elav) the RNAi against the
266 Drosophila ortholog Rpt5. Virgin females of Elav-Gal4 or the wild type 2U were crossed to
267 UAS-Rpt5 males. As standard in the field, we used 2 UAS-RNAi lines to rule out the

possibility of insertional or off-target effects. We included genetically appropriate controls with either UAS alone, Gal4 alone or the combination of Gal4 and UAS lines. For behavioural procedures, flies that were 0-2 days old were set up the day prior to testing and left in an incubator at 23°C with 40% humidity overnight. All testing occurred in an environmental chamber at 25°C with 70% humidity. Flies were given 1hr to acclimate to the environmental chamber prior to testing. First, Drosophila were trained to associate an odour with a foot-shock from classical olfactory conditioning as before [39]. Briefly, 100 flies are placed in a training chamber and provided with an odour (odour 1) (either octanol-OCT or methylcyclohexamide-MCH) that is presented simultaneously with a foot-shock for 60 seconds. After a brief airing, flies are then provided with a second odour (odour 2) without shock before finally being given a t-maze choice between the two odours for 2 minutes. Flies on each side of the t-maze are then counted. Then, a new set of 100 flies with the same genotype are trained to associate the other odour with a shock. A performance index is then calculated by calculating the ratio of flies avoiding the shocked odour to the total number of flies. For reversal learning, we used a similar approach to previous [40]. Reversal learning uses a similar set up and protocol with the added step of repeating the second odour 45s after it was first presented but this time paired with the shock, followed by the first odour without the shock 45s later, and finally the t-maze choice between the two odours. Statistical analysis was performed using ANOVA and then Tukey tests in JMP (SAS).

Data representation and statistical analyses

Data are typically mean ± SEM and analyzed by pair ratio t-test between two groups. All charts and statistical analyses were generated using GraphPad Prism version 8. A p-value <0.05 was considered significant. All data are available on request from authors.

Additional materials and methods are available in supplementary information

Results

Identification of *PSMC3* variants

The propositus, Subject #2, was a female newborn presenting with severe cardiac, gastrointestinal, inflammatory and immune issues. Whole-exome sequencing (WES) highlighted the *de novo* nonsynonymous c.523A>G p.(Met175Val) variant (GenBank ID: NM_002804.4), predicted to be pathogenic by bioinformatics programs and absent in any public variant databases (gnomAD, >246,000 chromosomes; NHLBI Exome Variant Server, >13,000 alleles; Bravo, 125,568 alleles). Via data sharing platform GeneMatcher [41] and direct requests in variants databases whose access was authorized to the University of Washington School of Medicine, a total of 14 distinct rare missense *PSMC3* variants could be identified *de novo* in 22 unrelated children presenting a syndrome characterized by neurodevelopmental delay (NDD) and various congenital anomalies **(Table 1)**.

As shown in **Figure 1A**, most of the *PSMC3* substitutions were localized in the "ATPases Associated with diverse cellular Activities" (AAA) domain and predicted to be intolerant to variations **(Figure S1)**. Two distinct regions of the AAA domain were particularly prone to substitutions. The first hotspot was centered on the recurrent variant c.910C>T p.(Arg304Trp) detected in four unrelated children and encompassed variants c.910C>G p.(Arg304Gly, c.915G>T p.(Glu305Asp) and c.929T>C p.(Met310Thr) **(Figure 1A)**. The second region enriched in rare variants [p.(Met259Thr), p.(Met259Val), p.(Ile261Thr) -seen six times-, p.(Gly262Arg) and p.(Arg269Pro)] was more N-terminally located **(Figure 1A)**. Importantly, all twelve affected residues were highly conserved across species from mammalians down to fission yeast **(Figure 1A)**.

One major phenotype hallmark of all individuals with *PSMC3* variants is the predominance of neurodevelopmental or neuropsychiatric symptoms **(Table 2)**. In more details, apart from Subject #2, all affected children had developmental delay (21/21; 100%) characterized by speech delay (18/18; 100%) and/or intellectual disability (15/17; 88%), and motor delay

(14/18; 78%). Brain magnetic resonance imaging highlighted frequent anomalies (11/14; 79%), whereas abnormal behavior (9/17; 53%) and seizures (5/20; 25%) were inconstant. 9/18 (50%) individuals experienced growth failure, with feeding difficulties (8/17; 47%). Malformations were frequently observed notably in skeleton (10/14; 71%; scoliosis, acetabular dysplasia, brachymetatarsy), heart (10/17; 59%; ventricular or septal defects, patent ductus arteriosus, pulmonary hypertension and atresia), kidney (4/14; 29%; horseshoe shape, pelvicalyceal dilatation, nephrocalcinosis, and multi-cystic dysplastic kidney), and head (microcephaly in 6/16 (38%); relative to severe macrocephaly in 2/16 (13%)). Tumors were noted in 2/18 (11%) individuals (craniopharyngioma and neuroblastoma). Hearing loss was detected in 8/18 individuals (44%) and labeled as sensorineural in two and conductive in one of them, respectively. Most children (17/19; 89%) displayed dysmorphic facial features, including notably tall or broad forehead (7/19; 37%), thin upper lip with down-turned corners of mouth (6/19; 32%), abnormal palate (5/19; 265/19; 26%), epicanthal folds (5/19; 26%), and orofacial clefts (2/19; 10%). Computational analysis of facial morphology by GestaltMatcher [42] revealed that facial dysmorphism among the *PSMC3* subjects was rather heterogeneous with similarities only observed between patients carrying identical variants **(Figure S2).**

***PSMC3*-silenced *Drosophila* adult flies fail to reverse stimulus contingencies**

Given the neuronal nature of the phenotype of *PSMC3* subjects, we next sought to address the potential involvement of *PSMC3* in cognitive function by evaluating the learning performance of Drosophila fruit flies with a knockdown of *PSMC3* (i.e. Rpt5) expression. To this end, we used a standard conditioning of odour-avoidance response in which animals were exposed to two different odours (OCT or MCH), only one of which resulting in the simultaneous application of a foot-shock (OCT+, MCH-), as previously described [39] **(Figure 2A)**. As shown in **Figure 2C**, pan-neuronal expression of Rpt5 RNAi resulted in no significant differences in learning performance for $Rpt5^{32422}$ (P=0.6435, N=4). Similarly, RNAi

expression in Rpt5^{53886} resulted in normal learning performance (P=0.5282, N=6) as well. We next determined the reversal learning performance of RPT5 silenced flies by training with an initial odour shock pairing (e.g. OCT+, MCH-) immediately followed by training with a reversed odour shock pairing (e.g. OCT-, MCH+) **(Figure 2B)**. Strikingly, reversal learning performance was significantly defective with pan-neuronal Rpt5 RNAi expression for Rpt5^{32422} (P<0.0001, N=4); the three control groups did not significantly differ from each other. RNAi expression also led to defective reversal learning performance for Rpt5^{53886} (P=0.0022, N=6); the three control groups once again did not significantly differ from each other **(Figure 2B)**. These data suggest that *PSMC3* appears as a prerequisite for the changes in learned associations.

Ectopic expression of PSMC3/Rpt5 or its variants differentially impact neuronal development

In view of the negative impact of *PSMC3* gene silencing on reversal learning, we next asked whether *PSMC3* was involved in the regulation of hippocampal neuron dendritic development. To address this point, we ectopically expressed wild-type *PSMC3* in murine primary hippocampal neurons prior to neurite length quantification, as previously described [43]. As shown in **Figure S3**, expression of wild-type *PSMC3* at an early developmental time point in vitro (Day In Vitro (DIV) 3) resulted in significantly reduced neurite length of the neurons when fixed 5 days later, at DIV8. These results indicate that increased levels of *PSMC3* is damaging for neuronal development. We next sought to determine whether the different *PSMC3* variants identified in NDD/ID patients behave differently compared to PSMC3 WT in neurons when ectopically expressed. Interestingly, expression of the p.(Arg304Trp), p.(Glu305Asp) and p.(Glu383Lys) variants resulted in similar neuronal morphological changes as seen with wild-type *PSMC3* **(Figure S3)**. By contrast, expression of the p.(Met175Val) variant did not affect neuronal morphology when compared to the empty vector control, and showed significant improvement when compared to wild-type *PSMC3*. Taken together these results suggest that *PSMC3* participates in the regulation of neurite

development and that any alteration of this gene might affect this process positively or negatively.

***PSMC3* variants differentially affect the Rpt5 steady-state protein level**

Because missense variants may cause haploinsufficiency by affecting mRNA and/or protein turnover, we next sought to determine the impact of the identified *PSMC3* variants on the Rpt5 steady-state expression level. To this end, nine *PSMC3* point variants were introduced in the SHSY5Y neuroblastoma cell line and expressed with a fused N-terminal HA tandem repeat prior to western-blot analysis. As shown in **Figure 3A**, four variants including p.(Arg171Trp), p.(Ala237Val), p.(Met259Val) and p.(Ile261Thr) had substantially lower steady-state protein levels than their wild-type counterpart. However, all *PSMC3* variants generated equivalent amounts of PSMC3 transcripts in SHSY5Y cells following a 24-h transfection **(Figure 3B)**, indicating that reduced expression at the protein level was due to increased protein turnover and/or decreased translation efficiency. Altogether, these data show that the *PSMC3* missense variants identified in NDD/ID subjects do not necessarily behave similarly.

***PSMC3* substitutions are predicted to affect inter and intra-molecular interactions between proteasome subunits**

We next attempted to predict the structural consequences of the each of the fourteen *PSMC3* substitutions by assessing the localization of the mutated residues in the human 26S proteasome structure generated by Dong et al. (PDB-entry code: 6MSK) [44]. As shown in **Figure 3C**, most of the affected amino acids emerge within the N-terminal α/β domain of PSMC3/Rpt5 with five residues (i.e. Gly262, Ile261, Met259, Arg304, Glu305) residing in two loops adjacent to the substrate tunnel pointing towards the center of the AAA-ATPase ring **(Figure 3D)**. Specifically, on one loop, Gly262 is fixed by a main chain hydrogen bond to Glu305, thereby promoting flexibility of the preceding loop containing Met259. Besides,

Glu305 itself is held through a salt bridge by Arg308 with its preceding residue Arg304 involved in a polar network stabilizing the neighbouring loop **(Figure S4)**. Because these six residues stabilize or are part of the tertiary structure of the loops, any alteration of these amino acids is predicted to affect substrate trafficking, as well as interactions with other AAA-ATPase subunits. As shown in **Figure S4**, the Ala237Val variant is more difficult to classify and does not reveal itself on structural level at first sight. However, one cannot exclude that the slight increase in residue size at position 237 might lead to structural changes. Indeed, our overexpression assays in SHSY5Y cells suggest that such substitution does affect sidechain packing and protein stability **(Figure 3A)**. The p.(Glu383Lys) missense variant is the only substitution lying within the C-terminal α-helical domain of PSMC3/Rpt5 adjacent to the 19S-20S interface. Interestingly, Glu383 holds Gln166 from the PSMA1/α6 subunit for polar interactions with both of the Arg169 and Arg386 residues **(Figure 3E)**. Variant of the negatively charged Glu383 to a positively charged Lys383 is therefore predicted to disrupt such hydrogen bond network and affect the association of the 19S complex with the 20S core particle. Interestingly, Glu287 is located in close proximity of the ATP binding site within PSMC3/Rpt5 **(Figure S4)** and its substitution into Gln287 presumably generates additional polar bonds with Asn333 likely to affect ATP binding and/or hydrolysis. As illustrated in **Figure S5**, Arg171 is positioned at the PSMC3/Rpt5-PSMC2/Rpt1 interface and is part of a polar network involving the neighboring Asp169 and Asn258 residues. As such, the substitution of positively charged arginine to hydrophobic tryptophan at this position is predicted to disrupt these interactions, and a fortiori to affect the contact between the two subunits **(Figure S5)**. As for the Met175Val residue, its change to Val175 results in the loss of a polarized thiol group and hydrophilic environment is likely to destabilize the tertiary structure of this protein region **(Figure S5)**. Taken together, these data suggest that the complex 26S proteasome structure could be strongly affected by the identified PSMC3/Rpt5 missense variants through distinct mechanisms including substrate translocation or 19S-ATPase-interaction with the 20S particle.

***PSMC3* variants differentially impact proteasome assembly in NDD/ID subjects**

To further address the pathogenicity of the *PSMC3* variants, T cells from Subjects #12, #17 and #20, were next analyzed by SDS-PAGE/western-blotting for their proteasome contents. As shown in **Figure 4A**, the expression levels of the proteasome α-subunits (i.e. α7) and PA28-α did not significantly vary between controls and index cases. Likewise, the abundance of the 19S subunits (i.e. Rpt5 and Rpn5) in mutant T cells was quite comparable to that detected in their control counterparts. Most importantly, none of *PSMC3* variant T cells showed reduced expression of the Rpt5 full-length protein, suggesting that proteasome dysfunction in these affected individuals was not due to haploinsufficiency.

T cells from affected individuals and relative controls (i.e. father and/or mother) were next analyzed for proteasome complex formation and activity by in-gel fluorescence or western blotting on native PAGE. As shown in **Figure 4B**, the chymotrypsin-like activity of the 26S and 20S proteasome complexes was reduced in Subjects #17 and #20, respectively, while it was mostly unchanged in Subject #12. Subsequent western-blot analysis revealed that the decreased 20S activity observed in Subject #20 was due to a decreased pool of her 20S-PA28 complexes, as determined by reduced band intensity for the α6 and PA28 proteins. In a similar fashion, a diminished expression of the α6, PSMC3/Rpt5 and PSMD12/Rpn5 subunits was observed in the 26S proteasomes of Subject #17 **(Figure 4B)**, indicating that the decline in 26S activity detected in this patient was likely to be attributed to decreased amounts of 26S complexes. However, the 20S and 26S proteasome pools of Subject #12 did not substantially vary when compared to those of his related control **(Figure 4B).** Altogether, these data indicate that both of the p.(Arg304Trp) and p.(Glu305Asp) PSMC3/Rpt5 variants critically affect 20S and/or 26S proteasome assembly in individuals with NDD/ID, while the p.(Gly262Arg) variant has little impact in this process.

Quantitative proteomics identifies specific biomarkers of *PSMC3* loss-of-function in NDD/ID subjects

To better understand the cellular consequences of *PSMC3* loss-of-function, we next performed a mass spectrometry (MS)-based comparative analysis of the proteome of Subjects #16 and #20 (p.Arg304Trp and p.Glu305Asp, respectively) to that of their wild-type counterparts. As shown in **Figure 5**, our data identified a protein biomarker signature consisting of seventeen ribosomal proteins of the small 40S (i.e. RPS) or large 60S (i.e. RPL) ribosomal subunits which were specifically upregulated in both investigated patients. This suggests that mRNA translation is a major affected pathway upon *PSMC3* loss-of-function, a notion which is further supported by the view that components of the mRNA processing machinery such as CELF1, LSM1, SSU72 and ITPA are also differentially expressed across patients and controls **(Figure 5)**. Other notable proteins whose abundances vary in *PSMC3* subjects include components of the immune system such as MX1 –a typical interferon (IFN)-stimulated gene product– and the α-chain of the IL3 receptor (IL3RA). Interestingly, these proteins are regulated in opposite directions with both patients exhibiting higher amounts of MX1 but reduced levels of IL3RA **(Figure 5)**. Our analysis further revealed that *PSMC3* loss-of-function was also associated with increased protein levels of the H1.5 and H1.2 linker histone H1 variants, a finding that may point to a distinct chromatin regulation in these patients. Collectively, these data suggest that patients with *PSMC3* variants exhibit alterations in basic cellular processes including mRNA translation, immune signaling and chromatin remodeling.

PSMC3 variants cause proteotoxic stress in patient cells

Control and subject T cells were next analyzed for their content in ubiquitin-protein conjugates by western-blotting. As shown in **Figure 6A**, all four investigated patients exhibited typical features of unbalanced protein homeostasis, as evidenced by increased accumulation of ubiquitin-modified species when compared to their respective related controls.

Proteotoxic stress is known to induce the unfolded and integrated stress response (i.e. UPR and ISR, respectively) [26]. To address this point, we monitored in both control and variant T cells from Subjects #12, #16, #17 and #20 the expression level of the GRP94 chaperone protein whose upregulation is understood to be a major hallmark of the UPR [45]. Indeed, as shown in **Figure 6A**, all four investigated *PSMC3* subjects exhibited increased steady-state expression levels of GRP94 when compared to their respective related controls, indicating that their T cells suffer from ER stress. However, the activation of the UPR was only partial, as the phosphorylation/activation status of two other UPR markers, namely IRE1 and eIF2α, was not changed between controls and *PSMC3* subjects **(Figure 6A)**. The failure to detect increased phosphorylated eIF2α is intriguing considering the fact that one its major upstream kinases, protein kinase R (PKR), was consistently activated in all subjects **(Figure 6A)**. It may however be easily explained by the observation that both eIF2α phosphatases GADD34 and CReP were consistently up-regulated across all four patients.

Interestingly, T cells with *PSMC3* variants were also endowed with increased steady-state expression levels of LC3-II **(Figure 6B)**, suggesting that the inability of these cells to eliminate ubiquitin-protein aggregates cells via their 26S proteasomes triggers a compensatory mechanism mediated by activation of the autophagy system. Consistently, the mitochondrial proteins PINK1 and Bnip3L/NIX were found to be decreased in all four NDD/ID subjects with *PSMC3* variants **(Figure 6B)**, supporting the notion that selective autophagic processes including mitophagy were persistently activated upon *PSMC3* disruption. Because proteasome impairment typically results in the release of the TCF11/Nrf1 transcription factor from the ER membrane [46, 47], we next sought to determine whether TCF11/Nrf1 was processed in NDD/ID affected individuals. However, no difference in the TCF11/Nrf1 processing pattern could be detected between controls and *PSMC3* subjects **(Figure 6B)**, suggesting that *PSMC3* variants associated with NDD/ID do not initiate the TCF11/Nrf1 signaling pathway.

T cells isolated from patients harboring *PSMC3* variants exhibit a typical type I IFN signature

Because proteasome loss–of–functions caused by variants in genes of 20S core particle subunits result in the generation of a typical type I IFN response [32], we next sought to determine whether alterations in the *PSMC3* gene would induce interferonopathies as well. To this end, we undertook a comparative examination of the mRNA levels of 750 predefined immunological relevant genes in T cells from *PSMC3* subjects and relative controls (father and/or mother) using the NanoString® nCounter platform. Interestingly, a total of 30 differentially expressed genes could be identified including 11 interferon-stimulated genes (ISG) which were specifically upregulated in all NDD/ID patients **(Figure 7A)**, suggesting that *PSMC3* loss-of-function is associated with a type I IFN response. Besides, our transcriptomic analysis of control and subject T cells further revealed that PSMC3 disruption resulted in the upregulation of genes of the notch signaling pathway such as NOTCH2 and JAG2 involved in neurodevelopment [48] **(Figure 7A)**.

To validate the type I IFN gene signature unraveled by our omics profiling of the *PSMC3* subjects, we next evaluated the transcription rate of six ISG (*IFI27*, *IFI44L*, *IFIT1*, *ISG15*, *RSAD2* and *IFI44*) by quantitative PCR in T cells isolated from these four families with *PSMC3* missense variants. Strikingly, as shown in **Figure 7B**, all four affected children (Subjects #12, #16, #17 and #20) exhibited much higher ISG expression levels than their parents (father and/or mother) used as controls. Calculation of the median fold change of the six ISG revealed that a minimum and significant increase of 2.23-fold was detected in all *PSMC3* index cases when compared to their respective controls. The strongest type I IFN signature was observed in Subject #17 whose ISG were upregulated by approximately 75- and 12-fold when compared to her father and mother, respectively. Subjects #12, #16 and #20 exhibited a milder type I IFN induction characterized by a 2-to 6-fold greater amount of ISG transcripts than their respective controls. Among the six ISG tested, IFIT1, and IFI44L

were the genes which underwent the most pronounced upregulation in all four NDD/ID affected individuals.

To strengthen our view that NDD/ID affected individuals with *PSMC3* missense variants develop an interferonopathy, we next calculated and compared the IFN scores of both *PSMC3* subjects and their related controls to those of T cells isolated from six healthy donors. As shown in **Figure 8**, three of the NDD/ID related controls had an IFN score slightly above the cut-off value of 2.466 defined by Rice et al. to be abnormal [49]. However, the IFN scores of all related and unrelated controls remain significantly lower than those of the four tested NDD/ID patients, thereby confirming that these *PSMC3* variants were associated with enhanced type I IFN signaling.

Discussion

Here, we report fourteen missense variants in the *PSMC3* gene in twenty-two unrelated individuals with NDD **(Figure 1, Tables 1 and 2)** which clearly identify the 19S AAA-ATPase proteasome subunit PSMC3/Rpt5 as a critical protein for the development of the central nervous system (CNS). This notion is in line with previous reports showing that conditional inactivation of other 19S proteasome subunits (i.e. PSMC1/Rpt2 and PSMC4/Rpt3) in mice results in severe neuronal phenotypes with features of neurodegeneration and locomotor dysfunction [50, 51].

Recently, a homozygous deep intronic variant creating a cryptic exon in the *PSMC3* gene was linked to a familial recessive neurosensory syndrome [52]. However, given their distinct modes of inheritance and pathogenesis, we believe that this recessive disorder observed in a single family and the dominant one, which we describe here in multiple families, are two different clinical entities. This assumption is substantiated by the fairly partial and inconstant overlap of disease phenotypes as neither cataract, nor neuropathy or similar cutaneous features –which are the hallmarks of the recessive syndrome- were observed in patients with NDD/ID reported in the present series. This notion is also supported by the fact that, unlike the familial recessive neurosensory syndrome described by Kroll et al., the dominant NDD/ID identified in this manuscript is not characterized by constitutive processing of TCF11/Nrf1 **(Figure 6B)**.

Cognitive flexibility is an important aspect of typical brain function which allows adaptation to both physical and social environmental changes [53, 54]. This may be assessed by evaluating reversal learning performance, a process which was identified several years ago in Drosophila adult flies [40] and whose dysfunction has been associated with the pathogenesis of various neuropsychiatric disorders [55-59]. Strikingly, while *PSMC3* gene-silencing in flies had no discernible effect on learning performance, it severely compromised reversal learning **(Figure 2)**. Interestingly, although proteasomes have been shown to

584 regulate long-term potentiation (LTP) [60, 61], their involvement in reversal learning was not
585 known. Our data clearly identify PSMC3/Rpt5 as a key regulator of this process whose
586 molecular landscape was initially limited to a few molecules related to the cytoskeleton and
587 GABAergic system [62-64]. Additional evidence in favour of a critical role of PSMC3/Rpt5 in
588 behavioural flexibility emerges from our experiments in primary hippocampal neurons
589 showing that PSMC3/Rpt5 overexpression affects dendrite growth **(Figure S4)**. One could
590 argue that the adverse effects of PSMC3/Rpt5 on this process might be due to extra-
591 proteasome functions as a consequence of an excess of "free" subunit following transfection.
592 However, our investigations on patient T cells clearly show that *PSMC3* missense variants
593 are associated with an increased accumulation of ubiquitin-modified proteins **(Figure 6A)**.
594 This indicates that these alterations give rise to proteasome loss-of-function variants
595 associated with perturbed protein homeostasis. Interestingly, our proteomic analysis
596 revealed that subject T cells carrying *PSMC3* variants were particularly enriched with
597 ribosomal proteins such as RPL4, RPL6, RPL7A and RPL7 **(Figure 5 and Table 3)**. These
598 proteins may be specifically targeted for degradation in these affected individuals and that
599 their accumulation occurs as a consequence of impaired intracellular protein clearance.
600 Consistent with this notion, proteasome inhibition has been recently shown to result in the
601 aggregation of ubiquitin-modified ribosomal proteins [65]. Our data therefore support the
602 recent view that ribosome dysregulation defines a key feature of NDD/ID phenotypes [66, 67]
603 and the concept of translational arrest upon proteotoxic stress via the action of eIF2a kinases
604 **(Figure 5A)**.
605
606 One key finding is the observation that NDD/ID subjects with *PSMC3* variants generate a
607 type I IFN gene signature with elevated expression of typical ISG including *IFIT1*, *IFI27*,
608 *IFI44*, *IFI44L*, *ISG15* and *RSAD2* **(Figures 7 and 8)**. Although it is well-established that
609 proteasome loss-of-functions variants cause interferonopathies in CANDLE/PRAAS subjects,
610 these alterations were long restricted to subunits of the 20S core particle and/or proteasome
611 assembly factors so far [29-35]. It was only recently that pathogenic variants in subunits of

the 19S regulatory particle, namely PSMD12, were reported to engage constitutive type I IFN signaling in patients with Stankiewicz-Isidor syndrome (STISS) (in press), a NDD disorder sharing levels of similarities with the one described in this manuscript. Intriguingly, although both CANDLE/PRAAS subjects and NDD/ID individuals with *PSMD12* or *PSMC3* variants carry genomic alterations that affect the same multi-subunit enzyme (*i.e*. 26S proteasome), their clinical phenotypes do not entirely overlap. Notably, NDD/ID subjects with *PSMC3* variants failed to develop recurrent fever, lipodystrophy and/or skin lesions which are usually detected in CANDLE/PRAAS subjects **(Table 1)**. One could argue that such differences may reflect distinct localizations of the affected subunits within the 26S proteasome complex, thereby suggesting that alterations of the 19S regulatory particle promote the generation of NDD/ID, while those of the 20S core particle and/or assembly chaperones favor the development a CANDLE/PRAAS phenotype. This assumption is however challenged by the fact that PSMB1/β6 variants of the 20S core particle lead to the acquisition of neuronal phenotype very similar to that seen in NDD/ID subjects with *PSMC3* variants [27]. The lack of systemic autoinflammation in NDD/ID subjects mounting a constitutive type I IFN response may seem surprising at first sight, but it is not totally unexpected, since this inconsistency is found in other neurodevelopmental disorders including Aicardi-Goutières [68, 69] and Down syndromes [70, 71]. This is particularly well exemplified in Down syndrome patients who, like NDD/ID subjects with *PSMC3* dominant variants, exhibit a constitutive activation of type I IFN signaling [72, 73]. To what extent type I IFN actively contributes to the pathogenesis of these disorders remains to be fully determined, even though a growing body of evidence supports the notion that IFN has detrimental effects on CNS function [74-77] and/or stem cell function and differentiation [78, 79].

Because proteasome dysfunction typically engages stress responses involving compensatory mechanisms such as autophagy [80], the integrated stress response (ISR) and the unfolded protein response (UPR) [26, 81], we reasoned that the sterile type I IFN response detected in subjects with *PSMC3* variants might be due to sustained activation of

either one of these pathways. As anticipated, high levels of autophagy and ER stress were detected in NDD/ID affected individuals, as evidenced by increased expression of the LC3-II and GRP94 proteins **(Figure 6A)**. Both PINK1 and NIX mitochondrial proteins were found to be decreased in NDD/ID subjects **(Figure 6B)**, suggesting that *PSMC3* variants increase autophagy-driven elimination of mitochondria (i.e. mitophagy). This observation supports the growing consensus that mitochondria dysfunction is a key determinant of the pathogenesis of neurodevelopment [82]. Besides, the activation status of PKR, a protein of the ISR that intersects with the UPR [83], was substantially increased in all investigated *PSMC3* subjects. Both ISR and UPR have the ability to counterbalance proteotoxic stress by inducing a global translational arrest via eIF2a phosphorylation. This is accompanied by concomitant accumulation of non-translated mRNAs, the formation of stress granules recruiting different RNA species and RNA processing enzymes, and IRE-1 dependent mRNA decay (RIDD) [84]. Although PKR typically responds to viral double stranded RNA [85], it also may undergo activation under sterile conditions upon different stresses including ER-stress involving PKR-associated activator PACT and its modulator TRBP, a protein required for micro RNA biogenesis [86-88]. Both, PACT and TRBP were observed to be increased in subject's cells along with a couple of RNA-processing factors in our omics analysis strongly indicating that PKR activation occurs via uncontrolled RNA processing. The mechanisms by which *PSMC3* variants activate PKR in NDD/ID affected individuals remain unclear, but our data open the possibility that PKR may sense a broader spectrum of danger signals than initially assumed, including perturbations of protein homeostasis. This concept is in line with the observation that activated PKR was found in the CNS of subjects with neurodegenerative diseases [89-92] and that neurodegeneration is associated with neuroinflammation [93, 94]. Altogether, our work demonstrates that heterozygous *PSMC3* dominant variants result in a neurodevelopmental syndrome associated with a specific type I IFN gene signature.

Acknowledgements

This work was supported by the German Research Foundation (SFBTR167, RGT2719-PRO project B4) to EK, E-Rare project GENOMIT (Austrian Science Fund FWF, I4695-B) to JAM, in part, by US National Institutes of Health (NIH) grants (R01MH101221) and a grant from the Simons Foundation (SFARI #608045) to E.E.E.; E.E.E. is an investigator of the Howard Hughes Medical Institute.

673 **References**
674
675 1. Tanaka, K., T. Mizushima, and Y. Saeki, *The proteasome: molecular machinery and*
676 *pathophysiological roles.* Biol Chem, 2012. **393**(4): p. 217-34.
677 2. Collins, G.A. and A.L. Goldberg, *The Logic of the 26S Proteasome.* Cell, 2017. **169**(5): p. 792-
678 806.
679 3. Toyama, B.H. and M.W. Hetzer, *Protein homeostasis: live long, won't prosper.* Nat Rev Mol
680 Cell Biol, 2013. **14**(1): p. 55-61.
681 4. Goloubinoff, P., *Mechanisms of protein homeostasis in health, aging and disease.* Swiss Med
682 Wkly, 2016. **146**: p. w14306.
683 5. Seifert, U., et al., *Immunoproteasomes preserve protein homeostasis upon interferon-induced*
684 *oxidative stress.* Cell, 2010. **142**(4): p. 613-24 PMID: 20723761.
685 6. Kruger, E. and P.M. Kloetzel, *Immunoproteasomes at the interface of innate and adaptive*
686 *immune responses: two faces of one enzyme.* Curr Opin Immunol, 2012. **24**(1): p. 77-83.
687 7. Pickart, C.M., *Mechanisms underlying ubiquitination.* Annu Rev Biochem, 2001. **70**: p. 503-33.
688 8. Demartino, G.N. and T.G. Gillette, *Proteasomes: machines for all reasons.* Cell, 2007. **129**(4):
689 p. 659-62.
690 9. Pickart, C.M. and D. Fushman, *Polyubiquitin chains: polymeric protein signals.* Curr Opin
691 Chem Biol, 2004. **8**(6): p. 610-6.
692 10. Pickart, C.M., *Back to the future with ubiquitin.* Cell, 2004. **116**(2): p. 181-90.
693 11. Tanaka, K., *The proteasome: overview of structure and functions.* Proc Jpn Acad Ser B Phys
694 Biol Sci, 2009. **85**(1): p. 12-36.
695 12. Dahlmann, B., *Mammalian proteasome subtypes: Their diversity in structure and function.*
696 Arch Biochem Biophys, 2016. **591**: p. 132-40.
697 13. Finley, D., *Recognition and processing of ubiquitin-protein conjugates by the proteasome.*
698 Annu Rev Biochem, 2009. **78**: p. 477-513.
699 14. Benaroudj, N., et al., *The unfolding of substrates and ubiquitin-independent protein*
700 *degradation by proteasomes.* Biochimie, 2001. **83**(3-4): p. 311-8.
701 15. Kisselev, A.F., W.A. van der Linden, and H.S. Overkleeft, *Proteasome inhibitors: an expanding*
702 *army attacking a unique target.* Chem Biol, 2012. **19**(1): p. 99-115.
703 16. Finley, D., X. Chen, and K.J. Walters, *Gates, Channels, and Switches: Elements of the*
704 *Proteasome Machine.* Trends Biochem Sci, 2016. **41**(1): p. 77-93.
705 17. Ebstein, F., et al., *Emerging roles of immunoproteasomes beyond MHC class I antigen*
706 *processing.* Cell Mol Life Sci, 2012. **69**(15): p. 2543-58 PMID: 22382925.
707 18. Strehl, B., et al., *Interferon-gamma, the functional plasticity of the ubiquitin-proteasome*
708 *system, and MHC class I antigen processing.* Immunol Rev, 2005. **207**: p. 19-30.
709 19. Shin, E.C., et al., *Proteasome activator and antigen-processing aminopeptidases are*
710 *regulated by virus-induced type I interferon in the hepatitis C virus-infected liver.* J Interferon
711 Cytokine Res, 2007. **27**(12): p. 985-90.
712 20. Tomko, R.J., Jr., et al., *Heterohexameric ring arrangement of the eukaryotic proteasomal*
713 *ATPases: implications for proteasome structure and assembly.* Mol Cell, 2010. **38**(3): p. 393-
714 403.
715 21. Smith, D.M., et al., *Docking of the proteasomal ATPases' carboxyl termini in the 20S*
716 *proteasome's alpha ring opens the gate for substrate entry.* Mol Cell, 2007. **27**(5): p. 731-44.
717 22. Greene, E.R., K.C. Dong, and A. Martin, *Understanding the 26S proteasome molecular*
718 *machine from a structural and conformational dynamics perspective.* Curr Opin Struct Biol,
719 2020. **61**: p. 33-41.
720 23. Greene, E.R., et al., *Specific lid-base contacts in the 26s proteasome control the*
721 *conformational switching required for substrate degradation.* Elife, 2019. **8**.
722 24. Verma, R., et al., *Role of Rpn11 metalloprotease in deubiquitination and degradation by the*
723 *26S proteasome.* Science, 2002. **298**(5593): p. 611-5.

25. Brehm, A. and E. Kruger, *Dysfunction in protein clearance by the proteasome: impact on autoinflammatory diseases.* Semin Immunopathol, 2015. **37**(4): p. 323-33 PMID: 25963519.
26. Ebstein, F., et al., *Contribution of the Unfolded Protein Response (UPR) to the Pathogenesis of Proteasome-Associated Autoinflammatory Syndromes (PRAAS).* Front Immunol, 2019. **10**: p. 2756 PMID: 31827472.
27. Ansar, M., et al., *Biallelic variants in PSMB1 encoding the proteasome subunit beta6 cause impairment of proteasome function, microcephaly, intellectual disability, developmental delay and short stature.* Hum Mol Genet, 2020. **29**(7): p. 1132-1143.
28. Agarwal, A.K., et al., *PSMB8 encoding the beta5i proteasome subunit is mutated in joint contractures, muscle atrophy, microcytic anemia, and panniculitis-induced lipodystrophy syndrome.* Am J Hum Genet, 2010. **87**(6): p. 866-72.
29. Arima, K., et al., *Proteasome assembly defect due to a proteasome subunit beta type 8 (PSMB8) mutation causes the autoinflammatory disorder, Nakajo-Nishimura syndrome.* Proc Natl Acad Sci U S A, 2011. **108**(36): p. 14914-9.
30. Kitamura, A., et al., *A mutation in the immunoproteasome subunit PSMB8 causes autoinflammation and lipodystrophy in humans.* J Clin Invest, 2011. **121**(10): p. 4150-60.
31. Liu, Y., et al., *Mutations in proteasome subunit beta type 8 cause chronic atypical neutrophilic dermatosis with lipodystrophy and elevated temperature with evidence of genetic and phenotypic heterogeneity.* Arthritis Rheum, 2012. **64**(3): p. 895-907.
32. Brehm, A., et al., *Additive loss-of-function proteasome subunit mutations in CANDLE/PRAAS patients promote type I IFN production.* J Clin Invest, 2015. **125**(11): p. 4196-211.
33. Poli, M.C., et al., *Heterozygous Truncating Variants in POMP Escape Nonsense-Mediated Decay and Cause a Unique Immune Dysregulatory Syndrome.* Am J Hum Genet, 2018. **102**(6): p. 1126-1142.
34. de Jesus, A.A., et al., *Novel proteasome assembly chaperone mutations in PSMG2/PAC2 cause the autoinflammatory interferonopathy CANDLE/PRAAS4.* J Allergy Clin Immunol, 2019. **143**(5): p. 1939-1943 e8.
35. Sarrabay, G., et al., *PSMB10, the last immunoproteasome gene missing for PRAAS.* J Allergy Clin Immunol, 2019.
36. Kury, S., et al., *De Novo Disruption of the Proteasome Regulatory Subunit PSMD12 Causes a Syndromic Neurodevelopmental Disorder.* Am J Hum Genet, 2017. **100**(2): p. 352-363.
37. Fonteneau, J.F., et al., *Generation of high quantities of viral and tumor-specific human CD4+ and CD8+ T-cell clones using peptide pulsed mature dendritic cells.* J Immunol Methods, 2001. **258**(1-2): p. 111-26.
38. Bolduc, F.V., et al., *Excess protein synthesis in Drosophila fragile X mutants impairs long-term memory.* Nat Neurosci, 2008. **11**(10): p. 1143-5.
39. Tully, T. and W.G. Quinn, *Classical conditioning and retention in normal and mutant Drosophila melanogaster.* J Comp Physiol A, 1985. **157**(2): p. 263-77.
40. Tully, T., et al., *Genetic dissection of memory formation in Drosophila melanogaster.* Cold Spring Harb Symp Quant Biol, 1990. **55**: p. 203-11.
41. Sobreira, N., et al., *GeneMatcher: a matching tool for connecting investigators with an interest in the same gene.* Hum Mutat, 2015. **36**(10): p. 928-30.
42. Hsieh, T.C., et al., *GestaltMatcher: Overcoming the limits of rare disease matching using facial phenotypic descriptors.* medRxiv, 2021. **medRxiv 2020.12.28.20248193**.
43. Kury, S., et al., *De Novo Mutations in Protein Kinase Genes CAMK2A and CAMK2B Cause Intellectual Disability.* Am J Hum Genet, 2017. **101**(5): p. 768-788 PMID: 29100089.
44. Dong, Y., et al., *Cryo-EM structures and dynamics of substrate-engaged human 26S proteasome.* Nature, 2019. **565**(7737): p. 49-55.
45. Marzec, M., D. Eletto, and Y. Argon, *GRP94: An HSP90-like protein specialized for protein folding and quality control in the endoplasmic reticulum.* Biochim Biophys Acta, 2012. **1823**(3): p. 774-87.

46. Steffen, J., et al., *Proteasomal degradation is transcriptionally controlled by TCF11 via an ERAD-dependent feedback loop.* Mol Cell, 2010. **40**(1): p. 147-58 PMID: 20932482.
47. Radhakrishnan, S.K., et al., *Transcription factor Nrf1 mediates the proteasome recovery pathway after proteasome inhibition in mammalian cells.* Mol Cell, 2010. **38**(1): p. 17-28.
48. Kostyszyn, B., et al., *Distribution of presenilin 1 and 2 and their relation to Notch receptors and ligands in human embryonic/foetal central nervous system.* Brain Res Dev Brain Res, 2004. **151**(1-2): p. 75-86.
49. Rice, G.I., et al., *Assessment of Type I Interferon Signaling in Pediatric Inflammatory Disease.* J Clin Immunol, 2017. **37**(2): p. 123-132 PMID: 27943079.
50. Bedford, L., et al., *Depletion of 26S proteasomes in mouse brain neurons causes neurodegeneration and Lewy-like inclusions resembling human pale bodies.* J Neurosci, 2008. **28**(33): p. 8189-98.
51. Tashiro, Y., et al., *Motor neuron-specific disruption of proteasomes, but not autophagy, replicates amyotrophic lateral sclerosis.* J Biol Chem, 2012. **287**(51): p. 42984-94.
52. Kroll-Hermi, A., et al., *Proteasome subunit PSMC3 variants cause neurosensory syndrome combining deafness and cataract due to proteotoxic stress.* EMBO Mol Med, 2020. **12**(7): p. e11861.
53. Reed, P., H. Watts, and R. Truzoli, *Flexibility in young people with autism spectrum disorders on a card sort task.* Autism, 2013. **17**(2): p. 162-71.
54. Leung, R.C. and K.K. Zakzanis, *Brief report: cognitive flexibility in autism spectrum disorders: a quantitative review.* J Autism Dev Disord, 2014. **44**(10): p. 2628-45.
55. Swainson, R., et al., *Probabilistic learning and reversal deficits in patients with Parkinson's disease or frontal or temporal lobe lesions: possible adverse effects of dopaminergic medication.* Neuropsychologia, 2000. **38**(5): p. 596-612.
56. Remijnse, P.L., et al., *Reduced orbitofrontal-striatal activity on a reversal learning task in obsessive-compulsive disorder.* Arch Gen Psychiatry, 2006. **63**(11): p. 1225-36.
57. Finger, E.C., et al., *Abnormal ventromedial prefrontal cortex function in children with psychopathic traits during reversal learning.* Arch Gen Psychiatry, 2008. **65**(5): p. 586-94.
58. Leeson, V.C., et al., *Discrimination learning, reversal, and set-shifting in first-episode schizophrenia: stability over six years and specific associations with medication type and disorganization syndrome.* Biol Psychiatry, 2009. **66**(6): p. 586-93.
59. Izquierdo, A. and J.D. Jentsch, *Reversal learning as a measure of impulsive and compulsive behavior in addictions.* Psychopharmacology (Berl), 2012. **219**(2): p. 607-20.
60. Smolen, P., D.A. Baxter, and J.H. Byrne, *Paradoxical LTP maintenance with inhibition of protein synthesis and the proteasome suggests a novel protein synthesis requirement for early LTP reversal.* J Theor Biol, 2018. **457**: p. 79-87.
61. Dong, C., et al., *Proteasome modulates positive and negative translational regulators in long-term synaptic plasticity.* J Neurosci, 2014. **34**(9): p. 3171-82.
62. Wilhelmsson, U., et al., *The role of GFAP and vimentin in learning and memory.* Biol Chem, 2019. **400**(9): p. 1147-1156.
63. Hausrat, T.J., et al., *Radixin regulates synaptic GABAA receptor density and is essential for reversal learning and short-term memory.* Nat Commun, 2015. **6**: p. 6872.
64. DePoy, L.M. and S.L. Gourley, *Synaptic Cytoskeletal Plasticity in the Prefrontal Cortex Following Psychostimulant Exposure.* Traffic, 2015. **16**(9): p. 919-40.
65. Sung, M.K., et al., *Ribosomal proteins produced in excess are degraded by the ubiquitin-proteasome system.* Mol Biol Cell, 2016. **27**(17): p. 2642-52.
66. Hetman, M. and L.P. Slomnicki, *Ribosomal biogenesis as an emerging target of neurodevelopmental pathologies.* J Neurochem, 2019. **148**(3): p. 325-347.
67. Bourque, D.K., et al., *A de novo mutation in RPL10 causes a rare X-linked ribosomopathy characterized by syndromic intellectual disability and epilepsy: A new case and review of the literature.* Eur J Med Genet, 2018. **61**(2): p. 89-93.

68. Crow, Y.J. and N. Manel, *Aicardi-Goutieres syndrome and the type I interferonopathies.* Nat Rev Immunol, 2015. **15**(7): p. 429-40.
69. Livingston, J.H. and Y.J. Crow, *Neurologic Phenotypes Associated with Mutations in TREX1, RNASEH2A, RNASEH2B, RNASEH2C, SAMHD1, ADAR1, and IFIH1: Aicardi-Goutieres Syndrome and Beyond.* Neuropediatrics, 2016. **47**(6): p. 355-360.
70. Araya, P., et al., *Trisomy 21 dysregulates T cell lineages toward an autoimmunity-prone state associated with interferon hyperactivity.* Proc Natl Acad Sci U S A, 2019. **116**(48): p. 24231-24241.
71. Waugh, K.A., et al., *Mass Cytometry Reveals Global Immune Remodeling with Multi-lineage Hypersensitivity to Type I Interferon in Down Syndrome.* Cell Rep, 2019. **29**(7): p. 1893-1908 e4.
72. Sullivan, K.D., et al., *Trisomy 21 consistently activates the interferon response.* Elife, 2016. **5**.
73. Sullivan, K.D., et al., *Trisomy 21 causes changes in the circulating proteome indicative of chronic autoinflammation.* Sci Rep, 2017. **7**(1): p. 14818.
74. Akwa, Y., et al., *Transgenic expression of IFN-alpha in the central nervous system of mice protects against lethal neurotropic viral infection but induces inflammation and neurodegeneration.* J Immunol, 1998. **161**(9): p. 5016-26.
75. Campbell, I.L., et al., *Structural and functional neuropathology in transgenic mice with CNS expression of IFN-alpha.* Brain Res, 1999. **835**(1): p. 46-61.
76. Kavanagh, D., et al., *Type I interferon causes thrombotic microangiopathy by a dose-dependent toxic effect on the microvasculature.* Blood, 2016. **128**(24): p. 2824-2833.
77. Goldmann, T., et al., *USP18 lack in microglia causes destructive interferonopathy of the mouse brain.* EMBO J, 2015. **34**(12): p. 1612-29.
78. Eggenberger, J., et al., *Type I interferon response impairs differentiation potential of pluripotent stem cells.* Proc Natl Acad Sci U S A, 2019. **116**(4): p. 1384-1393 PMID: 30606801.
79. Yu, Q., et al., *DNA-damage-induced type I interferon promotes senescence and inhibits stem cell function.* Cell Rep, 2015. **11**(5): p. 785-797 PMID: 25921537.
80. Zhu, K., K. Dunner, Jr., and D.J. McConkey, *Proteasome inhibitors activate autophagy as a cytoprotective response in human prostate cancer cells.* Oncogene, 2010. **29**(3): p. 451-62.
81. Studencka-Turski, M., et al., *Molecular Insight Into the IRE1alpha-Mediated Type I Interferon Response Induced by Proteasome Impairment in Myeloid Cells of the Brain.* Front Immunol, 2019. **10**: p. 2900 PMID: 31921161.
82. Khacho, M., R. Harris, and R.S. Slack, *Mitochondria as central regulators of neural stem cell fate and cognitive function.* Nat Rev Neurosci, 2019. **20**(1): p. 34-48.
83. Sadler, A.J. and B.R. Williams, *Structure and function of the protein kinase R.* Curr Top Microbiol Immunol, 2007. **316**: p. 253-92.
84. Reid, D.W., et al., *The unfolded protein response triggers selective mRNA release from the endoplasmic reticulum.* Cell, 2014. **158**(6): p. 1362-1374.
85. Meurs, E., et al., *Molecular cloning and characterization of the human double-stranded RNA-activated protein kinase induced by interferon.* Cell, 1990. **62**(2): p. 379-90.
86. Benkirane, M., et al., *Oncogenic potential of TAR RNA binding protein TRBP and its regulatory interaction with RNA-dependent protein kinase PKR.* EMBO J, 1997. **16**(3): p. 611-24.
87. Patel, R.C. and G.C. Sen, *PACT, a protein activator of the interferon-induced protein kinase, PKR.* EMBO J, 1998. **17**(15): p. 4379-90.
88. Siwecka, N., et al., *The Structure, Activation and Signaling of IRE1 and Its Role in Determining Cell Fate.* Biomedicines, 2021. **9**(2).
89. DeTure, M.A. and D.W. Dickson, *The neuropathological diagnosis of Alzheimer's disease.* Mol Neurodegener, 2019. **14**(1): p. 32.
90. Gal-Ben-Ari, S., et al., *PKR: A Kinase to Remember.* Front Mol Neurosci, 2018. **11**: p. 480.
91. Marchal, J.A., et al., *The impact of PKR activation: from neurodegeneration to cancer.* FASEB J, 2014. **28**(5): p. 1965-74.

877 92. Chukwurah, E., et al., *A tale of two proteins: PACT and PKR and their roles in inflammation.* FEBS J, 2021.
879 93. Muzio, L., A. Viotti, and G. Martino, *Microglia in Neuroinflammation and Neurodegeneration: From Understanding to Therapy*. Front Neurosci, 2021. **15**: p. 742065.
881 94. Ahmed, M.M., et al., *Innate Immune System Activation and Neuroinflammation in Down Syndrome and Neurodegeneration: Therapeutic Targets or Partners?* Front Aging Neurosci, 2021. **13**: p. 718426.

884

Table 1. Main characteristics of the *PSMC3* variants identified in the subjects included in the study.

Chromosomal localization (Chr11/GRCh37)	cDNA change *	Protein change	Inheritance	Variant database **	CADD Phred score (v1.6.)	MTR (FDR)	Metadome	MobiDetails ***	Number of subjects with the variant
g.47445677G>A	c.511C>T	p.(Arg171Trp)	*de novo*	rs775517283	27.3	0.573 (0.033)	I	45364	1
g.47445665T>C	c.523A>G	p.(Met175Val)	*de novo*	Absent	23.4	0.592 (0.062)	I	45365	1
g.47444406G>A	c.710C>T	p.(Ala237Val)	*de novo*	Absent	26.9	0.453 (0.015)	HI	45366	1
g.47444234T>C	c.775A>G	p.(Met259Val)	ND (suspected *de novo*)	Absent	23.4	0.564 (0.061)	I	45367	1
g.47444233A>G	c.776T>C	p.(Met259Thr)	*de novo*	Absent	24.7	0.564 (0.061)	I	45368	1
g.47444227A>G	c.782T>C	p.(Ile261Thr)	*de novo*	Absent	24.6	0.564 (0.061)	I	45369	6
g.47444225C>T	c.784G>A	p.(Gly262Arg)	*de novo*	Absent	26.8	0.626 (0.082)	I	45370	1
g.47444203C>G	c.806G>C	p.(Arg269Pro)	*de novo*	Absent	24	0.622 (0.046)	I	45371	1
g.47444150C>G	c.859G>C	p.Glu287Gln	*de novo*	Absent	26.7	0.645 (0.078)	I	45372	1
g.47442253G>A	c.910C>T	p.(Arg304Trp)	*de novo*	rs1363348500	31	0.392 (0.057)	I	45373	4
g.47442253G>C	c.910C>G	p.(Arg304Gly)	*de novo*	Absent	28.2	0.392 (0.057)	I	45374	1
g.47442248C>A	c.915G>T	p.(Glu305Asp)	*de novo*	Absent	23.1	0.357 (0.031)	I	45375	1
g.47442234A>G	c.929T>C	p.(Met310Thr)	*de novo*	Absent	26.2	0.387 (0.05)	HI	45376	1
g.47440729C>T	c.1147G>A	p.(Glu383Lys)	*de novo*	Absent	27.8	0.952 (0.843)	N	45377	1

* RefSeq transcript used for *PSMC3* is NM_002804.4 ; ** gnomAD V3, dbSNP v154, ClinVar v20210828 ; *** The access to detailed predictions for variant 2288X is as follows: https://mobidetails.iurc.montp.inserm.fr/MD/api/variant/453XX/browser/MTR= Missense Tolerance Ratio; FDR= false discovery rate; Metadome: I= intolerent; HI= highly intolerent; N= neutral

Table 2. Phenotype of subjects with *de novo PSMC3* variants (1/3)

Subject	**#1** [a]	**#2**	**#3** [b]	**#4**	**#5**	**#6**	**#7**
Variant in *PSMC3*	c.511C>T	c.523A>G	c.710C>T	c.775A>G	c.776T>C	c.782T>C	c.782T>C
	p.(Arg171Trp)	p.(Met175Val)	p.Ala237Val	p.(Met259Val)	p.(Met259Thr)	p.(Ile261Thr)	p.(Ile261Thr)
Gender	Male	Female	Male	Female	Male	Female	Female
Developmental delay	+	N/A	+	+	+	+	+
Speech delay	+	N/A	N/A	+	+	+	N/A
Facial dysmorphism	N/A	N/A	+	+	+	+	+
Intellectual disability	N/A	N/A	+	+	+	+	N/A
Brain MRI anomalies	N/A	+	N/A	N/A	-	+	+
Motor delay	N/A	N/A	N/A	-	+	+	+
Skeletal malformations	N/A	N/A	N/A	-	+	-	+
Gastrointestinal problems	N/A	+	N/A	-	+	-	-
Cardiac malformations	N/A	+	+	-	+	-	N/A
Hypotonia/abnormal tone	N/A	N/A	N/A	+	+	-	-
Abnormal behavior	+	N/A	N/A	-	+	+	-
Growth failure	N/A	+	N/A	-	-	-	-
Feeding difficulties	N/A	+	N/A	-	+	-	-
Hearing loss	N/A	N/A	N/A	+	+	-	-
Microcephaly	N/A	-	N/A	-	-	-	N/A
Other malformations	N/A	N/A	N/A	-	+	N/A	-
Genital abnormalities	N/A	N/A	N/A	-	+	-	-
Renal malformations	N/A	N/A	-	-	+	-	-
Seizures	N/A	-	+	-	+	-	-
Underweight	N/A	+	N/A	-	-	-	-
Short stature	N/A	-	N/A	-	N/A	-	-

* Nomenclature HGVS V2.0 according to mRNA reference sequence NM_002804.4. Nucleotide numbering uses +1 as the A of the ATG translation initiation codon in the reference sequence, with the initiation codon as codon 1.

N/A: parameter not analyzed; [a]information retrieved from 'Simons Foundation Powering Autism Research' (SPARK) cohort; [b]information retrieved from 'Deciphering Developmental Disorders' (DDD) cohort.

Table 2. Phenotype of subjects with *de novo PSMC3* variants (2/3)

Subject	**#8**	**#9**	**#10** [b]	**#11**	**#12**	**#13**	**#14** [b]	**#15**
Variant in *PSMC3*	c.782T>C	c.782T>C	c.782T>C	c.782T>C	c.784G>A	c.806G>C	c.859G>C	c.910C>T
	p.(Ile261Thr)	p.(Ile261Thr)	p.(Ile261Thr)	p.(Ile261Thr)	p.(Gly262Arg)	p.(Arg269Pro)	p.Glu287Gln	p.(Arg304Trp)
Gender	Male	Male	Male	Male	Male	Female	Male	Male
Developmental delay	+	+	+	+	+	+	+	+
Speech delay	+	+	+	+	+	+	N/A	+
Facial dysmorphism	+	+	+	+	-	N/A	+	+
Intellectual disability	+	+	+	+	-	+	N/A	+
Brain MRI anomalies	-	N/A	+	N/A	-	+	+	+
Motor delay	+	-	+	-	-	+	N/A	+
Skeletal malformations	+	N/A	+	-	N/A	N/A	N/A	+
Gastrointestinal problems	+	+	+	+	-	-	N/A	+
Cardiac malformations	-	N/A	-	-	+	N/A	+	+
Hypotonia/abnormal tone	+	+	+	-	-	+	N/A	+
Abnormal behavior	+	-	-	+	-	N/A	N/A	-
Growth failure	-	-	-	-	+	N/A	N/A	+
Feeding difficulties	-	-	-	+	-	N/A	N/A	+
Hearing loss	-	-	-	+	+	+	-	+
Microcephaly	-	-	N/A	-	-	N/A	N/A	+
Other malformations	-	-	+	-	N/A	N/A	+	-
Genital abnormalities	-	+	+	-	N/A	N/A	-	+
Renal malformations	N/A	N/A	N/A	-	N/A	N/A	-	+
Seizures	-	-	+	+	-	-	-	+
Underweight	-	-	-	-	+	N/A	N/A	-
Short stature	-	-	-	-	-	-	N/A	+

Table 2. Phenotype of subjects with *de novo PSMC3* variants (3/3)

Subject	**#16**	**#17**	**#18** [b]	**#19** [b]	**#20**	**#21**	**#22**	**Total (22 patients)**
Variant in *PSMC3*	c.910C>T	c.910C>T	c.910C>T	c.910C>G	c.915G>T	c.929T>C	c.1147G>A	
	p.(Arg304Trp)	p.(Arg304Trp)	p.(Arg304Trp)	p.(Arg304Gly)	p.(Glu305Asp)	p.(Met310Thr)	p.(Glu383Lys)	
Gender	Male	Female	Female	Female	Female	Male	Male	13M/9F
Developmental delay	+	+	+	+	+	+	+	**21/21 (100%)**
Speech delay	+	+	+	+	+	+	+	**18/18 (100%)**
Facial dysmorphism	+	+	+	+	+	-	+	**17/19 (89%)**
Intellectual disability	+	+	+	+	N/A	+	-	**15/17 (88%)**
Brain MRI anomalies	+	+	N/A	+	N/A	N/A	+	**11/14 (79%)**
Motor delay	+	+	+	+	+	+	+	**14/18 (78%)**
Skeletal malformations	+	+	N/A	+	+	-	+	**10/14 (71%)**
Gastrointestinal problems	+	N/A	N/A	-	-	+	+	10/17 (59%)
Cardiac malformations	+	+	+	+	N/A	-	-	10/17 (59%)
Hypotonia/abnormal tone	+	+	N/A	+	-	-	-	10/17 (59%)
Abnormal behavior	+	-	N/A	+	+	+	-	9/17 (53%)
Growth failure	+	+	+	-	+	+	+	9/18 (50%)
Feeding difficulties	+	+	N/A	+	-	-	+	8/17 (47%)
Hearing loss	+	+	N/A	-	-	-	-	8/18 (44%)
Microcephaly	+	+	+	-	+	+	-	6/16 (38%)
Other malformations	+	N/A	N/A	-	-	-	+	5/14 (36%)
Genital abnormalities	-	+	N/A	-	-	-	-	5/16 (31%)
Renal malformations	+	+	N/A	-	-	-	-	4/14 (29%)
Seizures	-	-	N/A	-	-	-	-	5/20 (25%)
Underweight	-	-	N/A	-	+	-	+	4/17 (24%)
Short stature	-	-	N/A	-	+	-	+	3/17 (18%)

Table 3. List of proteins enriched in *PSMC3* Subjects 16 and 20 versus their controls (mother and father/mother, respectively)

PG.Protein Groups	Protein name	Gene name	Mut/Co|signal_log2_ratio	Mut/Co|raw_p_value	Mut/Co|adjusted_p_value
P02749	Beta-2-glycoprotein 1	APOH	3,90875773	3,9233E-05	0,01752392
P01861	Immunoglobulin heavy constant gamma 4	IGHG4	3,41081457	3,9313E-07	0,0003951
Q02878	60S ribosomal protein L6	RPL6	3,09519982	8,1085E-05	0,02173071
P62424	60S ribosomal protein L7a	RPL7A	2,97520531	2,4946E-06	0,00143263
P18124	60S ribosomal protein L7	RPL7	2,90834996	5,5264E-05	0,01815176
P83731	60S ribosomal protein L24	RPL24	2,78639617	5,8732E-05	0,01815176
P16403	Histone H1.2	H1-2	2,72232694	4,4042E-05	0,0177049
P02768	Serum albumin	ALB	2,64236248	3,3722E-18	1,3556E-14
P36578	60S ribosomal protein L4	RPL4	2,50022766	3,276E-07	0,0003951
P01876	Immunoglobulin heavy constant alpha 1	IGHA1	2,32067402	3,007E-05	0,01511011
P20591	Interferon-induced GTP-binding protein Mx1	MX1	2,20162951	6,3215E-05	0,01815176
Q6P2Q9	Pre-mRNA-processing-splicing factor 8	PRPF8	1,33941179	1,5549E-06	0,00125012
Q01469	Fatty acid-binding protein 5	FABP5	-2,29088412	5,7962E-05	0,01815176

Figure Legends

Figure 1: Distribution of the *de novo* heterozygous PSMC3/Rpt5 variants and morphological abnormalities in subjects affected with NDD/ID. *A.* The localization of the 13 NDD-causing missense variants in the PSMC3/Rpt5 proteins are indicated in red. The AAA-ATPase domain of the PSMC3/Rpt5 proteasome subunit of the 19S regulatory particle is depicted in blue in the schematic representation. Pink circles indicate the presence of variants hotspots. Shown is also a sequence alignment of regions immediately adjacent to the amino acids subjected to missense substitutions. Comparison of the PSMC3 primary structure across six eukaryotic organisms indicates the high conservation of the missense variant residues identified in NDD patients which are highlighted by red boxes. ***B.*** Facial photos of affected subjects were withdrawn from the present version of the manuscript but can be accessed by querying GestaltMatcher database (https://db.gestaltmatcher.org/) using the term “PSMC3” in the gallery section.

Figure 2: Pan-neuronal disruption of PSMC3/Rpt5 results in normal learning performance but defective reversal performance. *A*. A T-maze, depicting standard conditioning of odour-avoidance response in which Drosophila flies are trained to avoid one particular odour chamber which is associated with a foot-shock (in this example, odour chamber 1). ***B***. Schematic illustration of the experimental timelines of the learning and reversal learning protocols used in these experiments. Reversal learning is assessed by reversing odour shock pairing (MCH-, OCT+), as indicated. ***C***. Upper left: no significant difference was detected in learning with pan-neuronal expression of Rpt5 RNAi for $Rpt5^{32422}$ (P=0.6435, N=4). Upper right: similarly, pan-neuronal expression of Rpt5 RNAi for $Rpt5^{53886}$ resulted in no significant difference in learning (P=0.5282, N=6). Lower left: reversal learning was significantly defective with pan-neuronal Rpt5 RNAi expression for $Rpt5^{32422}$ (P<0.0001, N=4). Lower right: pan-neuronal Rpt5 RNAi expression for $Rpt5^{53886}$ also resulted in significant learning defects (P=0.0022, N=6).

Figure 3: PSMC3/Rpt5 variants do not behave similarly at the molecular level. *A*. SHSY5Y cells were transfected with HA-tagged *PSMC3* mutants for 24 h prior to protein extraction and western-blotting using antibodies specific for PSMC3 and HA, as indicated. Both non-transfected and mock-transfected cells served as negative controls. Equal protein loading was ensured by probing the membranes with an anti-α-tubulin monoclonal antibody. Shown is one representative experiment out of two. ***B*.** SHSY5Y cells transfected with the various HA-PSMC3 variants were subjected to total RNA extraction followed by semi-quantitative RT-PCR using primer located in PSMC3 and the polyadenylation signal of the pcDNA3.1/*myc*-HIS expression vector (BGH). Equal loading between the samples was ensured by amplifying the RPL0 gene, as indicated. ***C*.** A sliced surface view of the 26S proteasome (grey) was superimposed with a cartoon representation of the subunits PSMC3/RPT5 (blue) and PSMB1/α6 (purple) as well as the substrate (orange). The ATP/ADP molecules of the AAA-ATPase ring are shown as green sticks, while the investigated missense variants as bright yellow spheres. ***D*.** Detailed representation of the missense variants in the loop region of the N-terminal α/β domain. Residues affected by variants are involved in a polar interaction network close to the substrate tunnel. ***E*.** Close up view on the RPT5-α6 interface affected by the p.(Glu383Lys) variant. Residues affected by variants are shown as bright yellow balls and sticks with atoms coloured by polarity (oxygen in red, nitrogen in blue and sulphur in dark yellow). Figures were created with PyMOL v. 2.0 (pymol.org) using the human 26S proteasome structure (PDB-entry code: 6MSK [44]).

Figure 4: PSMC3/Rpt5 variants cause proteasome assembly defects in individuals with NDD/ID. *A*. Five to twenty micrograms of RIPA lysates from T cells isolated from Subjects #12, #17 and #20 as well as related controls (index case's father and/or mother) were separated by SDS-PAGE followed by western-blotting using antibodies directed against PSMC3/Rpt5, PSMD12/Rpn5, PA28-α and Alpha7, as indicated. Equal protein loading was ensured by probing the membrane with an anti-α-tubulin antibody. ***B*.** Twenty micrograms of

native whole-cell lysates derived from T cells isolated from NDD Subjects #12, #17 and #20 as well as related controls (index case's father and/or mother) were separated by 3-12% native-PAGE prior to suc-LLVY-AMC in-gel activity assay to visualize the positions of the 20S and 26S proteasome complexes. Gels were subsequently transferred to blots and probed with antibodies specific for Alpha6, PSMC3/Rpt5, PSMD12/Rpn5 and PA28-α, as indicated.

Figure 5: Proteomic signatures of NDD/ID subjects carrying PSMC3/Rpt5 variants. Heatmap cluster analysis showing the similarities in the protein expression profiles of the *PSMC3* Subjects #16 and #20 (carrying the p.Arg304Trp and Glu305Asp *PSMC3* variants, respectively) compared to their related controls (father and/or mother of the proband), as indicated. Only the differentially expressed proteins with an absolute value of log2 fold-change greater than 2 were selected for the clustering analysis.

Figure 6: NDD/ID subjects carrying PSMC3/Rpt5 variants exhibit severe signs of protein homeostasis perturbations and alterations of the UPR, ISR and autophagy/mitophagy pathways. *A*. Five to twenty micrograms of RIPA lysates from T cells isolated from subjects #12, #16, #17 and #20 as well as related controls (*PSMC3* index case's father and/or mother) were separated by SDS-PAGE followed by western-blotting using antibodies directed against K48-linked ubiquitin-modified proteins, GRP94, IRE1, phospho-IRE1, eIF2α, phospho-eIF2α, GADD34, CReP, PKR, phospho-PKR and GAPDH (loading control), as indicated. ***B*.** RIPA-cell lysates from Subjects #12, #16, #17 and #20 as well as their related controls (*PSMC3* index case's father and/or mother) were subjected to SDS-PAGE/western-blotting using antibodies specific for LC3b, PINK1, BNIP3L and α-tubulin (loading control), as indicated.

Figure 7: NDD/ID subjects with PSMC3/Rpt5 missense variants exhibit a typical type I interferon (IFN) signature. *A*. Heat map clustering of gene expression in T cells isolated

from *PSMC3* subjects and their relative controls (father and/or mother of the proband). Each column represents one individual patient/related control and each row represents one gene. Clustering of genes and samples was carried out by centred Pearson correlation. Colour indicates normalized counts of each gene, with green representing higher expression and red relatively lower expression. ***B.*** Gene expression of six typical IFN-stimulated genes (*IFIT1*, *IFI27*, *IFI44*, *IFI44L*, *ISG15* and *RSAD2*) was assayed by RT-qPCR on T cells derived from the NDD/ID Subjects #12 (A), #16 (B), #17 (C) and #20 (D) as well as their respective controls (*PSMC3* index case's father and/or mother). Expression levels were normalized to GAPDH and relative quantifications (RQ) are presented as fold change over controls. Shown is also the median fold expression of the six ISG over relative controls. Statistical significance was assessed by ratio paired t test where *indicates $p<0.05$, ** indicates $p<0.01$ and *** indicates $p<0.001$.

Figure 8: Interferon (IFN) score of *PSMC3* subjects suffering from NDD/ID. IFN scores for the NDD/ID families #12, #16, #17 and #20 (related controls and affected individuals) as well as for six unrelated controls (1 to 6) were calculated as the median of the RQ of the six ISG over a single calibrator control. Shown are the IFN scores of each sample (left panel) and the sample groups i.e. related controls, unrelated controls and *PSMC3* subjects, as indicated (right panel). Statistical significance was assessed by ratio paired t test where *indicates $p<0.1$ and ** indicates $p<0.05$.

Figure 1

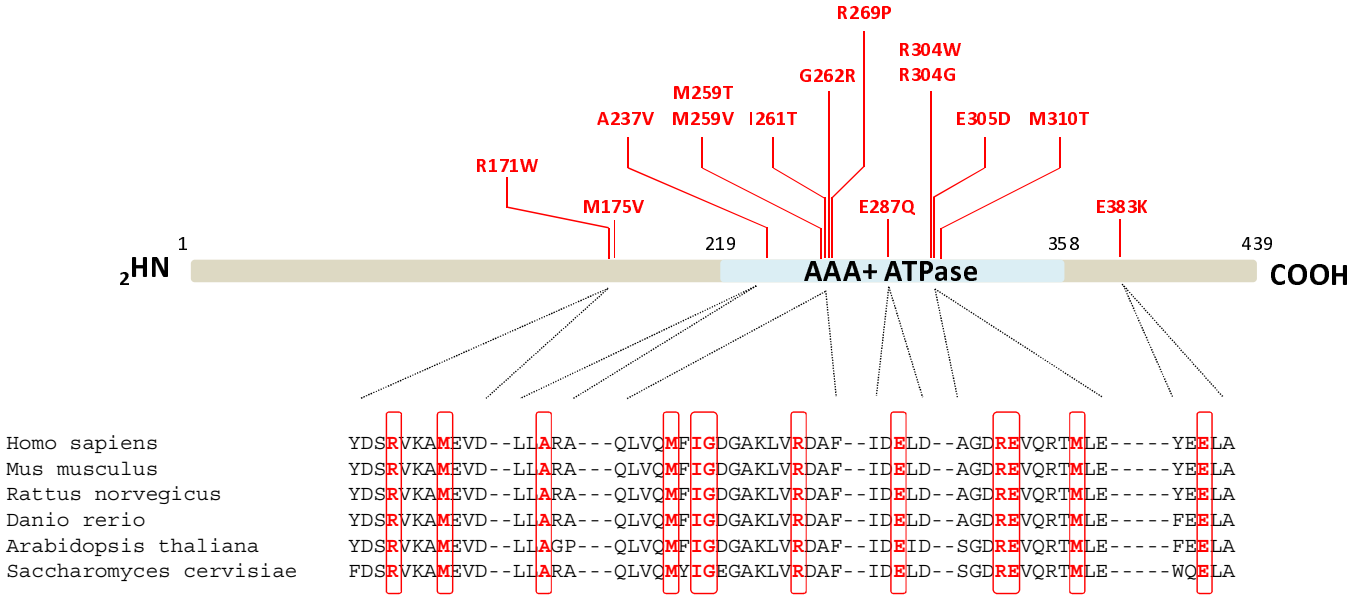

Figure 2

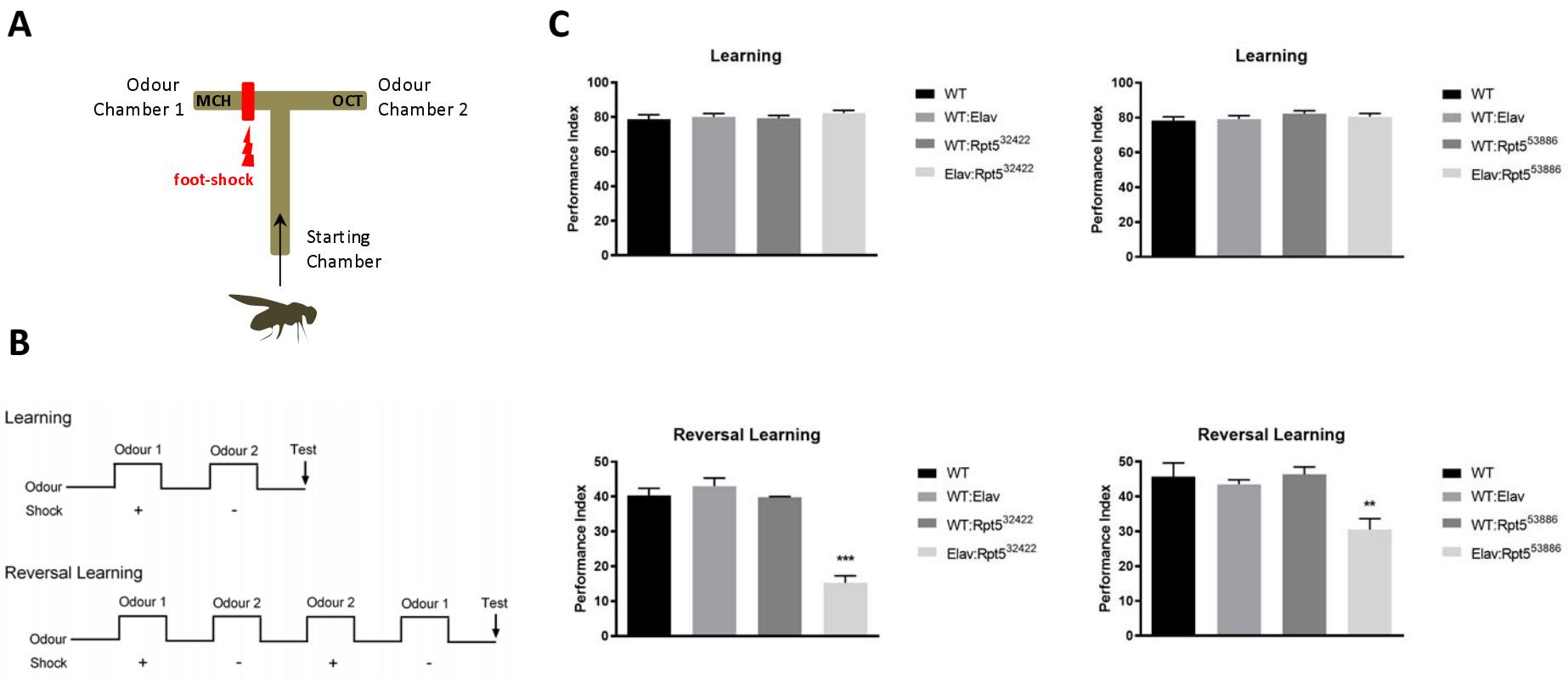

Figure 3

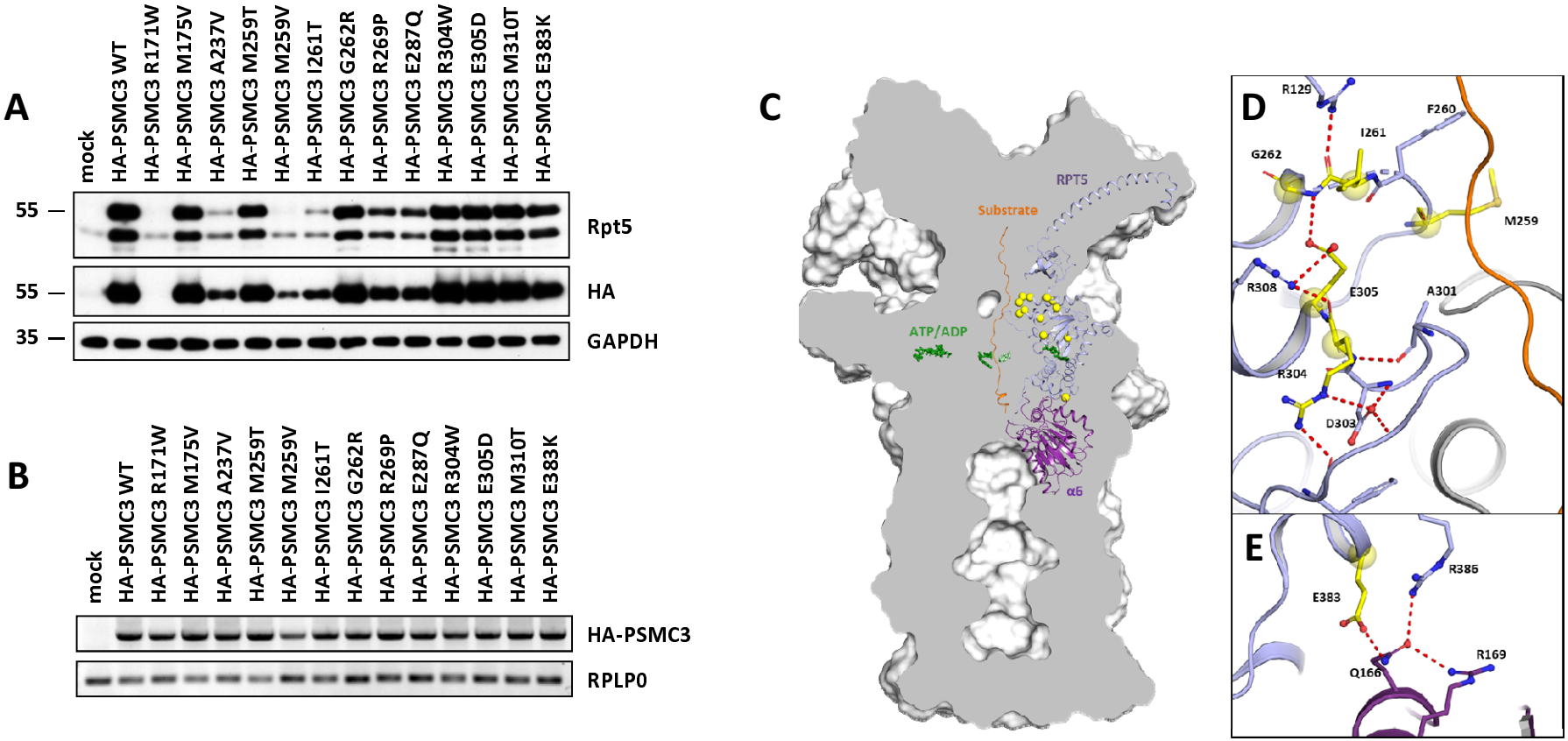

Figure 4

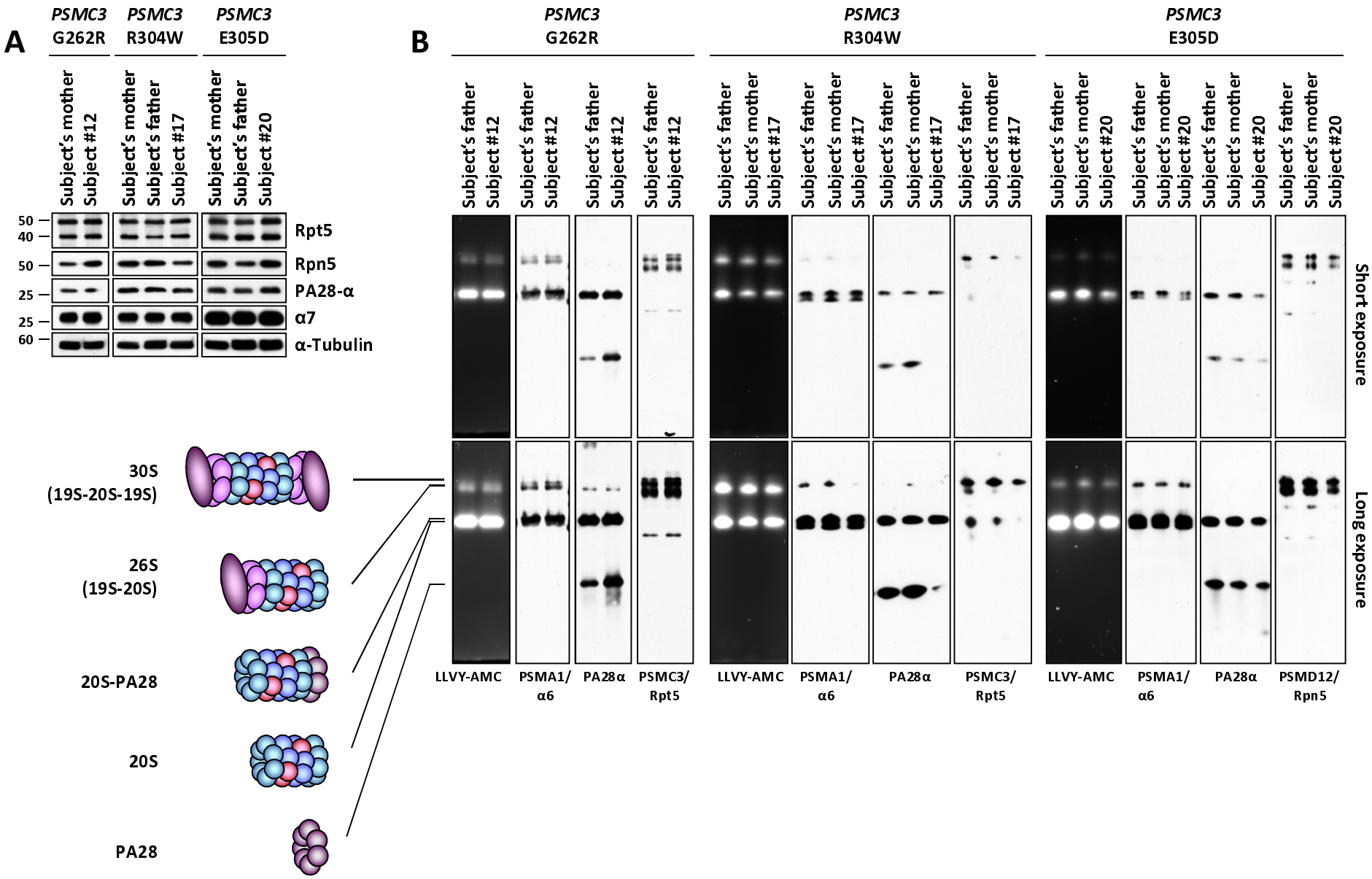

Figure 5

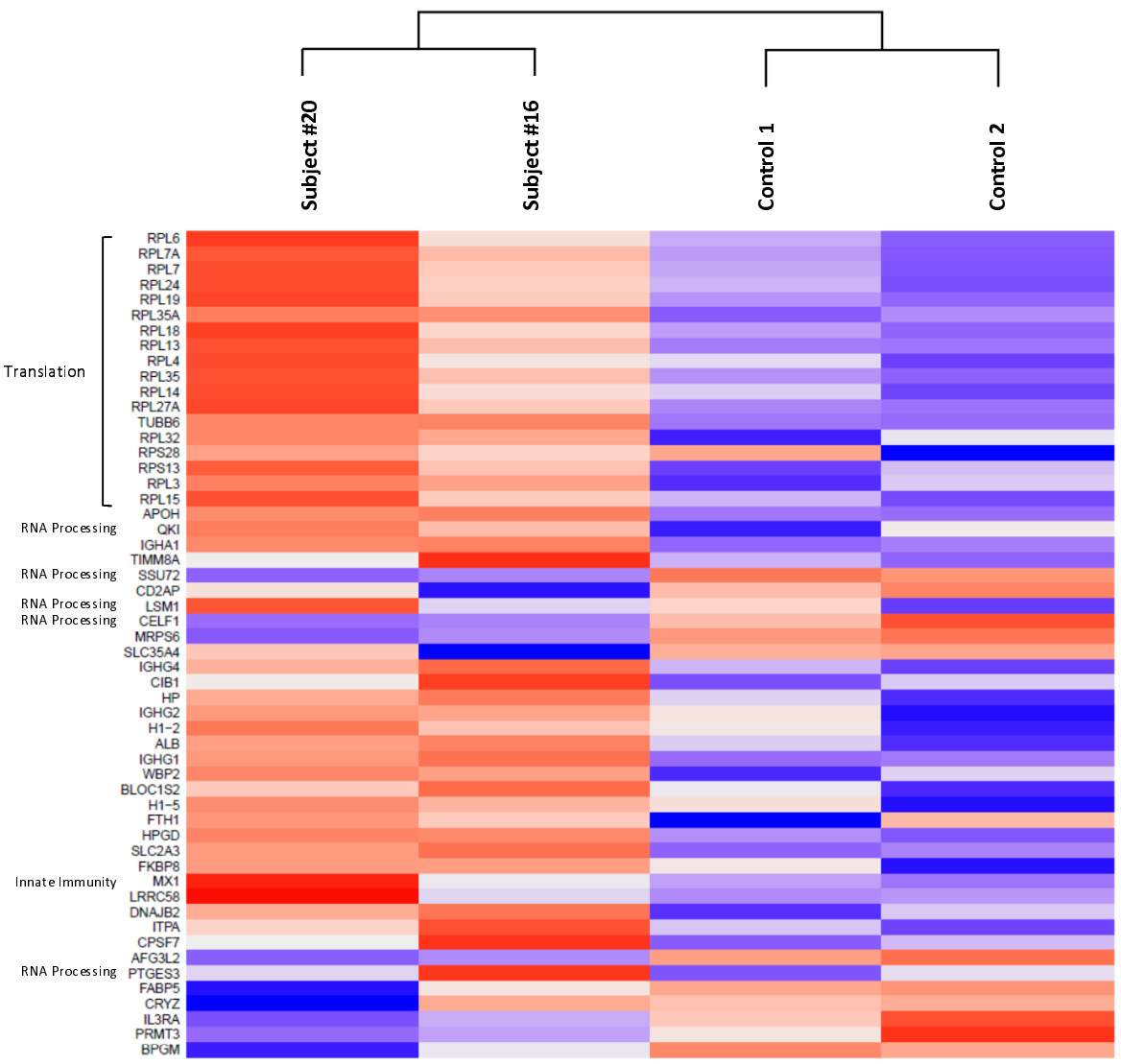

Figure 6

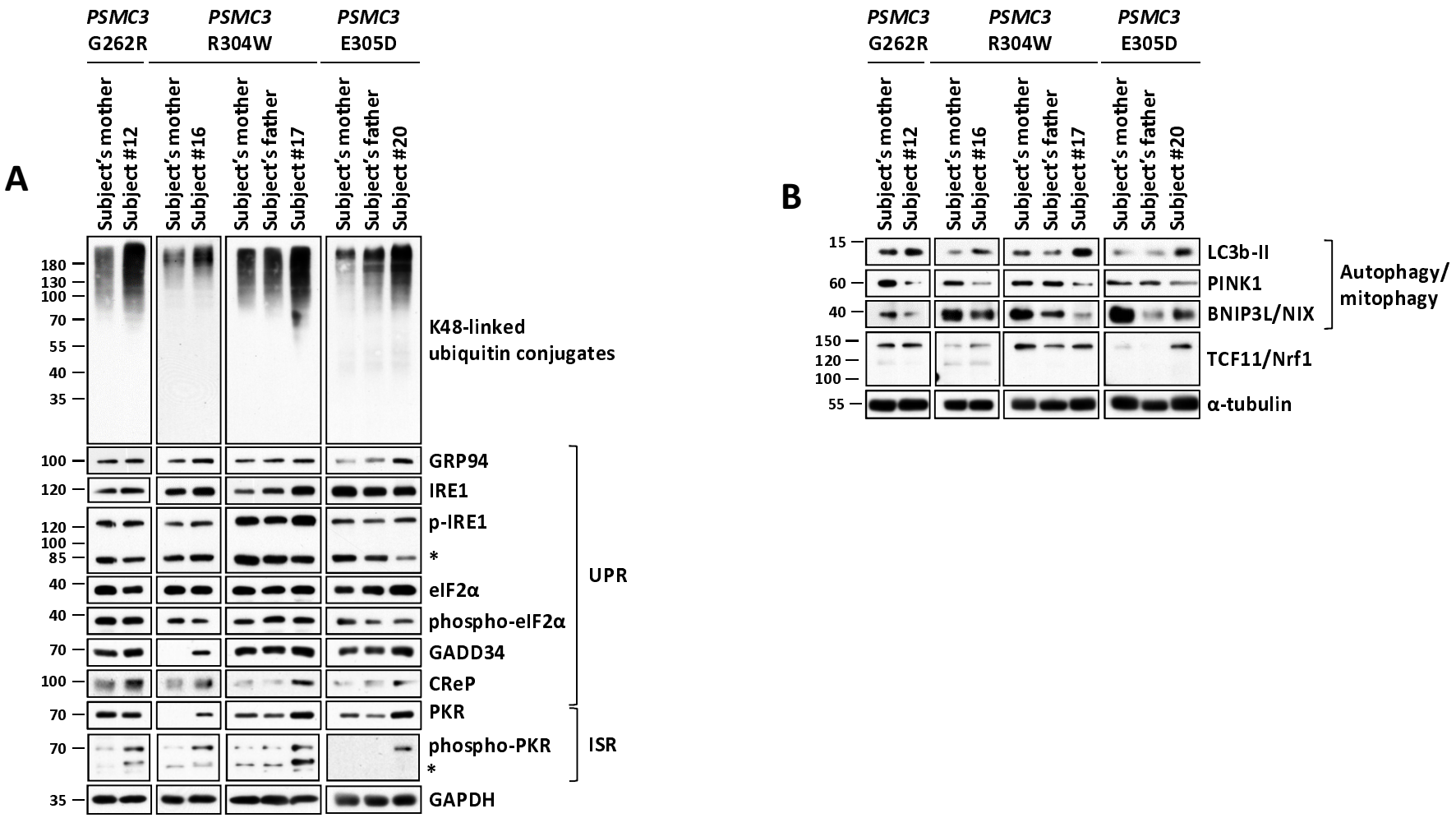

Figure 7

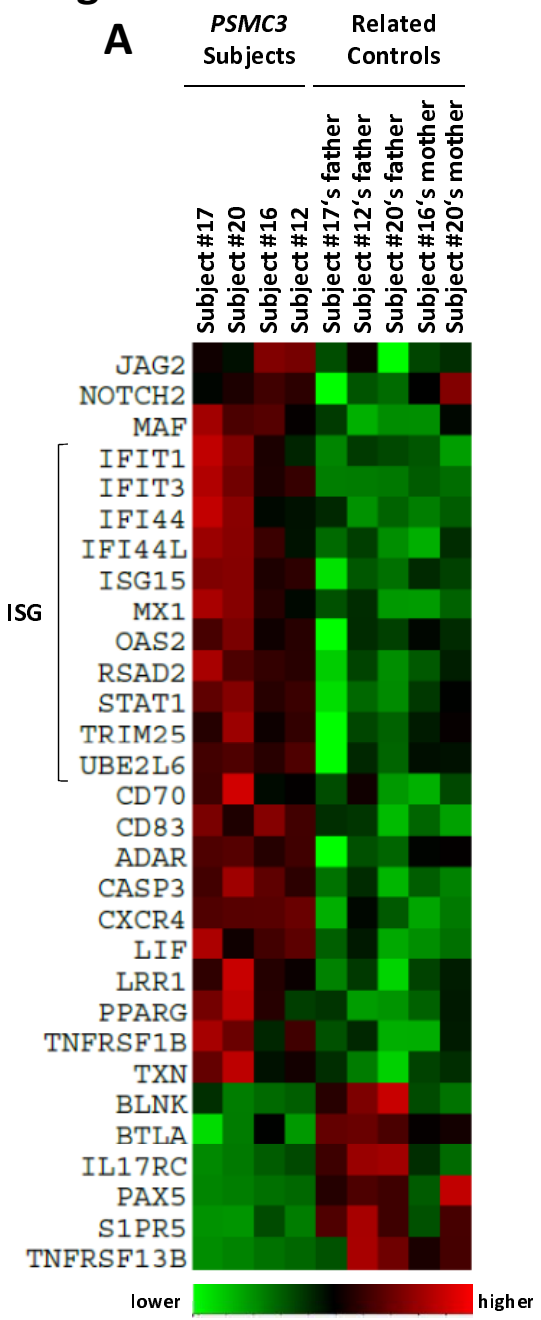

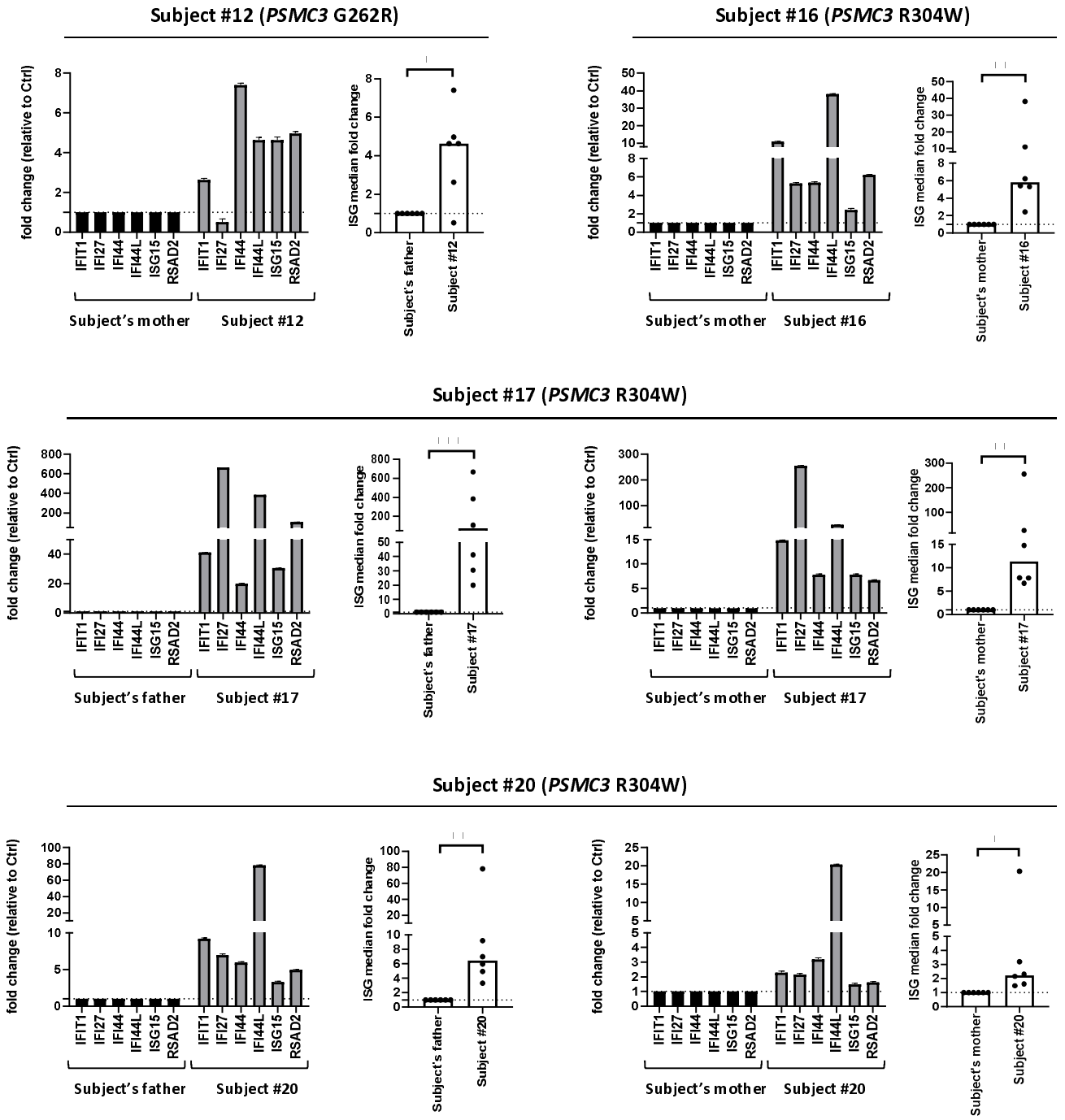

Figure 8